Review and Revision of the Lunar Cratering Chronology—Lunar Timescale Part 2

Stephanie C. Werner[1,2] , Benjamin Bultel[1,3] , and Tobias Rolf[1,4]

[1] Centre for Earth Evolution and Dynamics (CEED), Department for Geosciences, University of Oslo, Postboks 1028 Blindern, 0316 Oslo, Norway;
Stephanie.Werner@geo.uio.no
[2] Centre for Planetary Habitability (PHAB), Department for Geosciences, University of Oslo, Oslo, Norway
[3] now at: GEOPS Université Paris-Saclay, F-91400 Orsay, France
[4] Institute of Geophysics, University of Münster, D-48149 Münster, Germany
Received 2022 December 5; revised 2023 May 9; accepted 2023 May 10; published 2023 August 22

Abstract

Times and rates of planetary surface-modifying processes are crucial for the sequence and correlation of events on planetary bodies. For most planetary surfaces, superposition principles and crater densities are commonly used methods to collect relative age information. Lunar-based cratering-chronology models, which pair crater densities and sample ages from several lunar landing and sampling sites, calibrate the relative age information in absolute time. Here, we propose calibration pairs based on new crater statistics and spectrally supported sample-age assignments for the lunar cratering-chronology model. The resulting model reflects modern high-precision, radiometric ages, compositional and spectral information, and an up-to-date crater-production function. This revision supports a crater-forming projectile flux with monotonic decay, similar to previous standard models, but of distinctively lower flux. This originates from lower crater densities identified in spectrally and morphologically defined reference units, and from assigning more precise sample ages accounting for spectral resemblance between reference unit and sample. The observed maximal values for crater densities and ages provide the oldest and most densely cratered calibration pair. Because of the nature of highland samples, age constraints for the Luna 20 and Apollo 16 sampling sites remain challenging, which restricts the confidence in times for individual basin-formation events older than Orientale Basin. The new cratering-chronology model, when transferred to other planetary bodies, would cause aging of the surfaces, because of the lower overall flux.

Unified Astronomy Thesaurus concepts: Selenology (1441); Lunar science (972); Lunar impacts (958); Lunar surface (974); Lunar geochronology (954)

1. Why Is a Revision of the Lunar Cratering-Chronology Model Inevitable?

Lunar cratering-chronology models link observed crater densities with isotope geochemistry to produce time-calibrated stratigraphic sequencing of the Moon. Crater statistics result size-resolved and area-normalized crater frequencies and are the only tool to globally define the allocation of an extended geological unit to the temporal (time-stratigraphic) system of the respective planetary body. The models are calibrated with lunar mission samples and are considered a template for the temporal evolution of the projectile flux in the inner solar system.

Since the Apollo and Luna missions, crater counts have been remade (e.g., Robbins 2014), crater-production functions have been modified (e.g., Ivanov 2001), sample ages have been revised by updates for new decay-constant values (e.g., Michael et al. 2018), and new ages have been acquired on samples using instrumentation with improved accuracy and precision (e.g., Nemchin et al. 2021). Recently, a sample return of the Chang'E 5 mission added a new calibration point (Li et al. 2021; Che et al. 2021). Therefore, the existing lunar cratering-chronology models need revision to account for these developments. One of the current standard cratering-chronology models (i.e., Neukum 1983) uses primarily averaged radiometric ages for the model calibration obtained prior to

1981, which are summarized in the "Study on Basaltic Volcanism on the Terrestrial Planets" (Basaltic Volcanism Study Project 1981, Table 7.3.1). These ages are no longer accurate after several updates of the radioactive decay-rates used in radiometric dating techniques. Furthermore, global spectral mapping has become available at different wavelengths and high resolution (e.g., Jolliff et al. 2000; Gillis et al. 2004; Pieters et al. 2009; Paige et al. 2010). These spectral data allow a better constraint of reference units (e.g., Werner et al. 2022) and to improve links of the crater densities to sample type, composition, and absolute age. In this work, we present a new set of N_{cum}–age pairs for the chronology calibration. N_{cum} is the normalized cumulative-crater frequency for a defined crater diameter determined by counting craters on reference units. These reference units as here presented are mapped by Bultel & Werner (2023) using spectral data in relation to sample composition; the spectra-based assessment of samples and sites provides the assignment of sample ages for the age.

The global history and stratigraphy of the Moon have been comprehensively described in Wilhelms (1987). The ages measured for the different samples or in lunar meteorites provide dates for their crystallization and potential heating events (including impact melting and breccia formation), and the cosmic-ray exposure reveals the residence time at the lunar surface. Compared to meteorites, the advantage of samples is that their collected sites are seemingly well known. Geochemically, the lunar samples separate into two major classes: those that could have formed during volcanic activity, basaltic rocks and glasses, found by Apollo 11, 12, 14, 15, 16, 17; Luna 16, 20, 24; and now Chang'E 5; and those resulting from impact
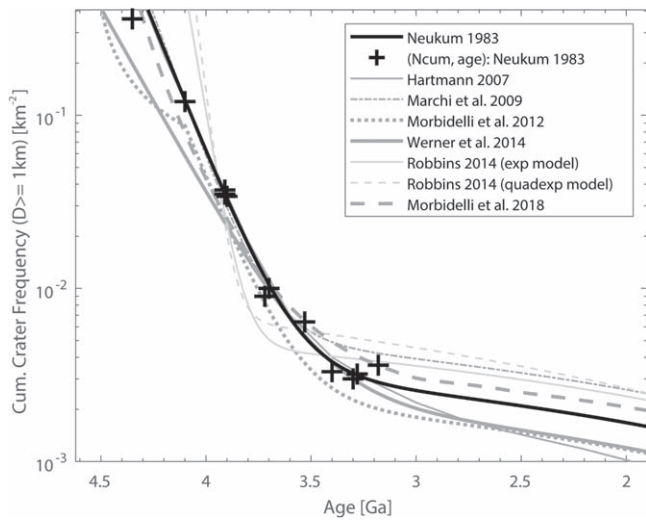
Figure 1. Several cratering-chronology models for cumulative-crater frequencies with diameter D greater or equal to 1 km. Here, we display only the calibration points from Neukum (1983) using black crosses. For defining their models, Marchi et al. (2009); Morbidelli et al. (2012, 2018), Werner et al. (2014) reinterpreted existing crater size–frequency measurements by Neukum (1983), while Hartmann et al. (2007), Robbins (2014) collected their own crater size–frequency measurements to provide calibration points.

bombardment, impactites, most with highland-composition affinity (Apollo 14, 15, 16, 17; and Luna 20). The impactites are mostly impact breccia composed of lithic and mineral clasts derived from continuous comminution due to impact bombardment of the original lunar crust and its different rock types, primarily of anorthositic composition, since the formation of the Moon. Overall, these ages enable constraining selenological events that occurred on and in the Moon, and thus set the lunar stratigraphy in an absolute timeline.

Both impact bombardment and potentially volcanic activity continue at low intensity until the present day. Details on the intensity of volcanism and bombardment have been debated, depending on the exact ages used for different rocks and cratering-chronology models, and partly because samples may have been transported farther, and meteorite source coordinates remain unknown. A global temporal assessment using crater statistics and as such a chrono-stratigraphy is reliable only when the applied cratering-chronology model is well-constrained and up-to-date. The correlation between samples collected during the Apollo and Luna missions and their respective stratigraphic unit remained often unclear, and does not exist for meteorites. Traditionally, sample ages have been used for dating basin formation or local lava emplacement. The relationship between samples and impact basins has been a matter of debate since the 1970s and translated into various definitions for the impact-basin and crater-forming projectile flux in the solar system. Figure 1 shows a nonexhaustive collection of cratering-chronology models, which depict either a slow, monotonic decay of the impact flux since at least the Moon formation (e.g., Neukum 1983) or a single spike in the flux (lunar terminal cataclysm, Tera et al. 1974; late heavy bombardment, Wetherill 1975; "saw-tooth" cataclysm, Turner et al. 1973; Morbidelli et al. 2012), but also hybrid versions such as a spiky decaying flux (Tera et al. 1974; Hartmann 2003; Fernandes et al. 2013; heavy bombardment eon, Fritz et al. 2014).

The diversity is due to the challenge of linking samples collected at highland sites to a source. The material collected on these sites is affected by impact gardening due to subsequent impacts (i.e., breaking and mixing of the material on the lunar surface into ever smaller particles, from boulder size to μm-size particles as a result of continued impact bombardment, Arvidson et al. 1975). Even after about 50 yr, many of the basin-formation ages remain debated.

Presently, there seems to be greater consensus regarding the age of Imbrium Basin (e.g., Nemchin et al. 2021) using compositional affinity of the samples collected at the Apollo 14 and 15 sites and the Procellarum KREEP terrain (PKT). This is challenged by the samples recently returned by Chang'E 5 from the PKT that lack the KREEP-enriched component (Li et al. 2021; Tian et al. 2021). Furthermore, Werner et al. (2022) reported a stratigraphic relationship of Apollo 14 samples with Orientale instead of Imbrium Basin, so that the same samples discussed by Nemchin et al. (2021) would rather date Orientale and not Imbrium. Reassessing all sample sites further changes the derivation of the solar system projectile-flux estimates. Covering a similar period, today, there exist calibration pairs of crater densities and ages for Mars (Farley et al. 2014; Werner et al. 2014; Werner 2019), but calibration still relies fundamentally on the sample collection from the Earth's moon for which numerous samples exist to derive the small-body flux or cratering-chronology models. The 50th anniversary of the Apollo sample acquisition missions, the most recent sample return from Chang'E 5, and the meanwhile collection of several spectral data sets motivated us to revisit sample information and mapping of the landing sites, which prompted a revision of the lunar cratering chronology as outlined in the following.

2. Data and Methods

The preparation of cratering-chronology models requires various inputs to enable an analytical description for linking ages of rock samples and crater statistics. To perform the measurements of the areal density of craters, a reference unit needs to be outlined that is uniform in age and spectrally matches sample composition as close as possible. One needs to understand the stratigraphy of the site and the relation to the representative samples for the calibration age. The stratigraphic relationships at the sites may be built from sequential deposition of globally distributed basin ejecta, but also can be mixed during small-scale, regional cratering activity.

2.1. Reference Units and Image Data

For our task of determining and interpreting the local crater densities and linking sample ages, we used units that show the landing site spectral characteristics. We follow Bultel & Werner (2023), who outlined sample-based geological units for each landing site using Apollo and Luna sample composition and spectral information. Thereby, they vetted the remote-sensing spectral mapping and sample affinity. Bultel & Werner (2023) evaluated the spectral information of the pixel at the actual landing site coordinates for absorption features indicating the presence of olivine, pyroxene, distinguished in high- and low-calcium pyroxene, feldspar and/or spinel. That work used recent spectral data provided by the hyperspectral imager (Goswami & Annadurai 2009) of the Moon Mineralogy Mapper (M^3; Green et al. 2011) Instrument that flew on board the Chandrayaan-1 mission by the Indian

Space Research Organisation. Further detailed analysis compared the spectral site characteristics with the sample composition reported in the literature and with infrared spectra of Apollo and Luna samples provided through the RELAB spectral library (NASA RELAB facility at Brown University, RELAB collection).[5] Based on the comparison between the near-infrared measurements performed on Apollo and Luna samples with their remote-sensing investigation, Bultel & Werner (2023) matched the sample and landing site spectral and compositional characteristics and used these common compositional features to define the respective count units. These maps, which display regional variation of the detection criteria, are provided as a color-composite image for each landing site. A specific color indicates the spectral feature detection, and their similarities and differences across and beyond the landing-site reference unit. The full set of composite maps of Bultel & Werner (2023) is collected in supplementary Figure A1. The count units used in our investigation thereby demark homogeneous and consistent units based on spectral investigation. This investigation also defines the sample (group) that is most representative, which furthermore specify the sample-related ages.

Using the landing-site units defined by Bultel & Werner (2023), we performed all crater size–frequency measurements in this analysis using terrain camera images of the Japan Aerospace Exploration Agency led Kaguya/Selene mission (Haruyama et al. 2008), available via the SELENE data archive.[6] We processed the Selene/Kaguya image data using the USGS Integrated Software for Imagers and Spectrometers (ISIS3,[7]) and imported all data sets into ArcGIS. The spatial image resolution of 10 m per pixel allowed us to count with confidence craters with diameters greater than 200 m. Both lunar morning and evening mosaics were used to perform the crater counts. This enhances the probability of recognizing shallow craters and measuring their diameters accurately.

2.2. Crater Statistics

Crater statistics are used as a measure of relative age. The cratering-chronology model is to provide absolute ages and describes surface exposure to the bombardment of impact crater-forming projectiles. The number of projectiles increases with decreasing size. For deriving absolute ages from crater densities, it is assumed that the shape of the projectile size–frequency distribution curve does not change through time, and a so-called crater-production function can be defined. The often-normalized crater density shifts to higher values, the longer the surface is exposed to the flux of projectiles. This statistical measure allows comparing the relative age of surfaces across the Moon, and links rock-stratigraphy to a time-stratigraphy (for a review see Werner & Ivanov 2015). A prerequisite is the mapping of reference units (geologically, spectrally, or any other map-defining criteria) so that the units represent a single emplacement event in time. However, the description of a geological uniform unit may in detail be more complex. Lava plains may be built of several flows with little to substantial time passing between each event. These flows may not resurface the entire counting area, which will be reflected in the crater record by small or large offset features (i.e., kinks) in

the cumulative size–frequency plots or frequency drops in incremental size–frequency plots when compared to an isochron (crater-production function for a specific age). Other geological processes, such as erosion, may widen small craters (Ivanov 2017; Xie et al. 2017). This effect could manifest by a steepening of the crater size–frequency distribution (CSFD) with increasing age of the surface. A crater-counting technique and the various methods of display have been defined by the Crater Analysis Techniques Working Group (1979) and are commonly used to represent the number of craters (sorted in bins of diameters) observed on a given unit of known surface areal size.

In this study, given the image resolution and the size of the counting units, the crater record measured is commonly representative of craters larger than 200 m in diameter (smaller for Chang-E 5 and Luna 24), while the largest crater measured is variable for the different areas. The upper crater diameter is limited due to either the size of the area or the age of the investigated unit. We use the cumulative description for the CSFD plots and crater-production function best fits using a nonlinear least-squares algorithm (Levenberg 1944; Marquardt 1963) to derive a normalized crater density. Depending on the successful unit outline, the observed CSFD should represent a single age of the last surface-forming event. For the evaluation of the observed CSFDs, we use the updated crater-production function suggested by Ivanov (2001), thereby following earlier work by Werner et al. (2014). We report eventually occurring resurfacing of the reference units according to deviations from the production function. We utilize the in-built resurfacing correction of the CraterStats tool (Michael & Neukum 2010) required for best fits in cumulative distribution plots to obtain the resurfacing related crater frequency and extrapolate when needed to reference crater densities such as the cumulative number of craters with diameters equal and larger than 1 km ($N_{cum}(D \geqslant 1\ [km])$), accordingly. We caution that such extrapolations depend on the crater-production function; see the discussion in Section 4.1. For several landing sites, we do not observe single-event curves in agreement with the complex sample-age ranges. Relevant processes are resurfacing by lava or ejecta emplacement, but also impact gardening, erosion, and potentially saturation, according to an empirical equilibrium (Hartmann 1984), related to subsequent crater formation.

2.3. Site Calibration Ages

Since earlier cratering-chronology model proposals (e.g., Neukum 1983), which for example averaged existing sample ages (Basaltic Volcanism Study Project 1981), new ages have been determined for Apollo and Luna mission samples. Thus, the utilized sample ages need updating to improve on the past averaging approach and because the decay constants for two isotope systems have been revised since then. For the ^{40}K decay constant needed for $^{40}Ar/^{39}Ar$ dating, modern values are suggested by Schwarz et al. (2011), Renne et al. (2011), updating those by Steiger & Jäger (1977). Additionally, the ages of several of the neutron fluence-monitors used in $^{40}Ar/^{39}Ar$ have been reevaluated (Jourdan et al. 2006; Jourdan & Renne 2007; Schwarz & Trieloff 2007). Similarly, the ^{87}Rb-decay constant has been revised several times (Steiger & Jäger 1977; Minster et al. 1982; Nebel et al. 2011; Rotenberg et al. 2012). Thus, it is unlikely that any of the ages used in the calibration by Neukum (1983) are still accurate, but not all

---

sample ages can be updated due to lack of detailed information. The resulting corrected ages do not change systematically, which is depending on the original decay constant and monitor used. Fortunately, a large number of new ages have been obtained since 1981 (Basaltic Volcanism Study Project 1981), especially in recent years using uranium–lead or lead–lead dating.

As discussed in Section 1, samples may have been transported farther, and meteorite source coordinates remain unknown, but also samples themselves may be aggregates. Breccia have a varying matrix composed of fused regolith material. Furthermore, it was pointed out early on that lunar sample nomenclature lacks systematics and causes confusion (Walker et al. 1973), which still persists. The sample collection reveals that the more samples are investigated the greater is the diversity in rock types, making it challenging to assign a precise reference age for the sites. Therefore, spectral data guided our sample choice in addition to rock type and composition. In this work, we chose the recommended age based on the convergence of sample bulk composition recognizable in sample near-infrared spectra and the respective site remote-sensing data obtained by the Moon Mineralogy Mapper (M^3) on board Chandrayaan-1. We discuss the age choice for each site below.

2.4. Derivation of the Cratering-Chronology Model

Cratering-chronology models describe the accumulation of craters (as N_{cum}, normalized cumulative-crater frequency) through time. The calibration of the chronology models base on crater frequencies at the different landing sites with corresponding radiometric age data. Over the last several decades, a number of different models (some shown in Figure 1) have been derived using these N_{cum}–age calibration pairs (some shown in Figure 1), all of which seem to agree within a factor of 2 or 3. Although most current models have different functional forms, they essentially suggest that the crater-forming projectile flux has been much higher in the early solar system compared to today, and that the decay may have been rather rapid within the first 1.5 billion years.

The cumulative impact rate must capture the impact probability of today's projectile population and satisfy the calibration pairs for the past. Neukum (1983) used the combination of an exponential decay and a constant flux term to build the equation that captures the flux through time. Integration allows for the description of the total crater accumulation through time, which is the cratering-chronology model.

2.5. Global Basin Ejecta Distribution: Predicted Landing Site Stratigraphic Columns

Samples have been attributed to large basins, implying that their basin ejecta have been deposited at the sampling sites and stayed preserved in the local stratigraphic column. As detailed in Werner et al. (2022), we computed the distribution of basin ejecta (Figure 2) across the lunar surface to derive a pseudo-stratigraphy at each landing site and to build virtual drill cores. Our computation is based on a simple scaling law (Zhu et al. 2015; Rolf et al. 2017) that determines the thickness of ejecta per basin at an angular distance away from the basin center depending on the basin size. For the parameters, especially the ones that control how fast the ejecta thickness decreases with

increasing distance from the rim, we stayed consistent with those used in previous studies (e.g., McGetchin et al. 1973; Fassett et al. 2011). For the basin diameters, we follow Neumann et al. (2015).

The total stratigraphy is then given by the superposition of layers originating from the different basins following the sequence derived by Fassett et al. (2012). Younger ejecta are emplaced on top of older contributions, but inside a newly formed impact basin, the stratigraphy is set to zero in our model, for simplicity. The basin may be filled afterwards with ejecta deposits from younger impact basins. Basin diameters may be ambiguous. Although we follow Neumann et al. (2015) for the crater diameters, it is not fully understood for multiringed basins, whether the previous interior surface and thus its crater record would be reset due to mare infill in the entire interior. Most obvious is this discrepancy for the Luna sites, which appear to be interior to the Crisium Basin rim, but surface morphology indicates that Luna 16 landed on Mare Fecunditatis adjacent to Crisium Basin, Luna 24 clearly inside Crisium Basin on Mare Crisium, while Luna 20's position is found in between on highland materials. As discussed in Werner et al. (2022), our simple modeling approach has several limitations and uncertainties, for instance related to oblique impacts and directions as well as to mixing of ejecta with the target material before deposition (e.g., Oberbeck 1975). The obtained pseudo-drill cores shall therefore not be used for an accurate description of lunar stratigraphy, but nevertheless provide useful upper bounds for layer thicknesses. We used these stratigraphic columns to identify major depositional contributions at relevant landing sites and the relative proportions or likely presence of basin ejecta material in the sample collection. Table 1 summarizes the predicted stratigraphic columns of basin ejecta for the investigated sampling sites. Furthermore, we indicate those sites that are blanketed due to more recent lava emplacement.

3. Resulting Calibration Pairs per Landing Sites

For all landing-site units, we collect crater diameters and locations to determine frequency values and crater densities, and we compared our observed CSFD obtained to results from units reported by Neukum (1983), reinterpreted by Marchi et al. (2009), and observed by Robbins (2014). The calibration reference crater frequency is derived by fitting an isochron based on the production function suggested by Ivanov (2001). Each landing site and adjacent units were characterized using spectral analysis of the M^3 data sets (Bultel & Werner 2023), and images aided to extract distinct morphological features. For defining the reference units related to the sample sites, the remote-sensing observations were compared with what is known from samples. Based on these analyses, Bultel & Werner (2023) defined the outlines for uniform reference units (supplementary figure A1), and we here follow the similarity evaluation that defines the sample for the reference age. In the following, we report the observations and recommend revisions per landing site for previous calibration frequency–age pairs for Apollo 11, 12, 14–17, as well as Luna 16 and 24. We also extend the calibration to the previously not reported Luna 20 site and the newest site sampled by Chang'E 5. We start with the youngest and newest site and proceed by increasing age.
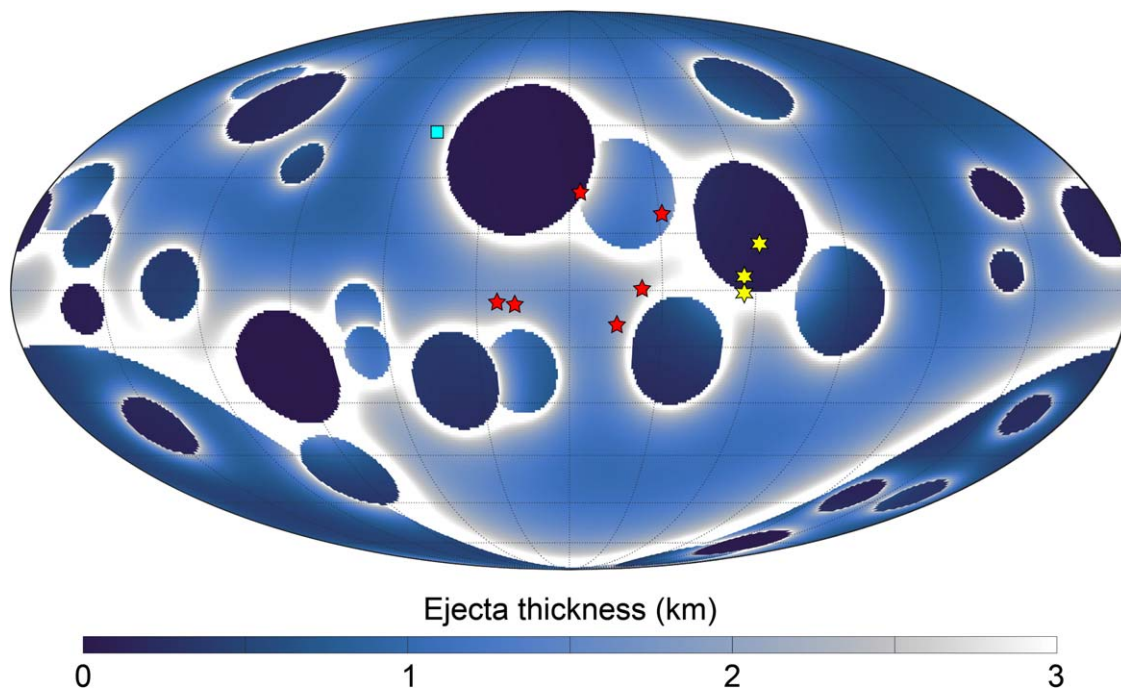
Figure 2. Modeled distribution of basin ejecta across the lunar surface assuming basin diameters suggested by Neumann et al. (2015). Pentagrams indicate the six Apollo sampling sites, while hexagrams indicate the three Luna sampling sites, and the square indicates the Chang'E 5 sampling site. The distribution is representative once basin formation has ceased (i.e., after the Orientale formation), but does not account for subsequent resurfacing due to lava emplacement that formed the maria.

Table 1
Ejecta Contribution (in Meters) of Different Basins to the Lunar Landing Site Stratigraphy

	A11	A12	A14	A15	A16	A17	L16	L20	L24	C5
Grimaldi	2	14	10	*3*	2	*1*	1	*1*	*1*	*10*
Nubium	50	564	745	*34*	119	*19*	12	*11*	*8*	*13*
Humboldtianum	9	3	4	*14*	5	*22*	14	*17*	*30*	*25*
South Pole-Aitken	119	150	145	*69*	147	*82*	160	*146*	*131*	*93*
Crüger-Sirsalis	1	12	8	*2*	2	*1*	1	*1*	*1*	*5*
Coulomb-Sarton	3	5	4	*6*	2	*4*	2	*2*	*3*	*4*
Humorum	28	426	299	*29*	49	*15*	10	*9*	*7*	*25*
Serenitatis	591	87	111	*Reset*	240	*Reset*	124	*145*	*142*	*56*
Smythii	39	8	9	*17*	28	*46*	318	*310*	*387*	*5*
Nectaris	1142	49	66	*72*	1085	*204*	546	*401*	*167*	*11*
Mendel-Rydberg	3	9	8	*3*	5	*2*	2	*2*	*2*	*~0*
Crisium	293	32	39	*127*	138	*825*	2700	*Reset*	*Reset*	*24*
Imbrium	237	531	519	*Reset*	204	*361*	76	*83*	*85*	*Reset*
Schrödinger	1	~0	~0	*~0*	1	*~0*	1	*1*	*1*	*~0*
Orientale	8	33	27	*11*	11	*6*	4	*4*	*3*	*30*
Total Ejecta	2533	1933	2002	394	2045	1599	3979	1143	979	2075
Mare Emplacement	Yes	Yes	⋯	Yes	⋯	Yes	Yes	⋯	Yes	Yes

Note. The ejecta contribution for the basins are as shown in Figure 2. Basins (except Schrödinger) that contribute only less than 2 m at the sites are omitted in this table, but included in the total sum. "Reset" indicates that the previous ejecta contribution (printed in italic) should not be visible in the present stratigraphy since preexisting (older) layers were destroyed by the new basin formation, or covered by its substantial ejecta. Subsequent contributions could be present in the sample collection, unless further mare lava emplacement covers the site.

3.1. Chang'E 5

The first Chinese sample-return mission landed in 2020 in the Northern Oceanus Procellarum east of Mons Rümker on a volcanic plain. This plain is part of the so-called PKT and has been identified as one of the youngest mare units based on crater statistics (e.g., Hiesinger et al. 2000). The site thus allows sampling of the young volcanic activity of the most recent part of Eratosthenian period (e.g., Qian et al. 2018). Although clearly of volcanic origin, mapping the craters of this area is particularly challenging, because it is covered with crater clusters in the diameter range of interest (e.g., Wu et al. 2018). Some effort has been put into linking these clusters to distant source craters (Qian et al. 2021). The here-proposed reference unit avoids these crater clusters and is limited to the local surrounding of the landing site.

3.1.1. Chang'E 5: Crater Statistics Review and New Results

Since it is a new calibration opportunity after about 50 years, multiple studies have performed crater counts for this site (e.g., Qian et al. 2021, 2018; Wu et al. 2018). The cumulative-crater
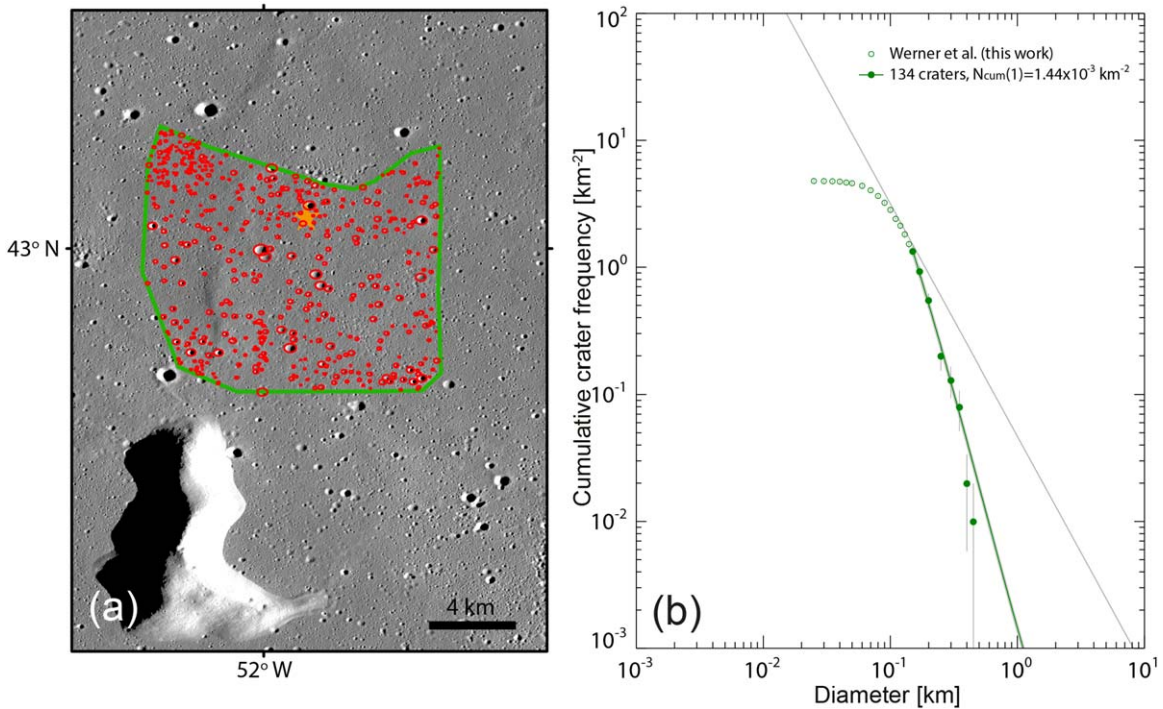
Figure 3. Crater statistics for the Chang'E 5 landing area. (a) Counting unit with craters, the star marks the actual landing site. (b) The respective crater size–frequency distribution and the saturation empirical equilibrium (gray solid line, after Hartmann 1984).

frequencies $N_{cum}(D \geqslant 1$ km$)$ range between $1.21 * 10^{-3}$ and $1.74 * 10^{-3}$ km^{-2} (compare also to Figure 4 in Li et al. 2021). All studies confirm a low crater density and a young age of the area, but the variability shows its contamination with crater clusters indicative of secondary craters that do not reflect the projectile flux of the formation period. We therefore worked with a much smaller unit surrounding the landing site. The areal size is 100 km^2, and we cover a crater-diameter range that includes craters smaller than 500 m. We use only craters above 150 m in diameter for the determination of the cumulative-crater frequency; because, at lower diameters, the slope of the CSFD resembles that for a saturated crater population in empirical equilibrium (Hartmann 1984). We can fit a single isochron to the above-described crater range (Figure 3), with a resulting cumulative calibration-crater frequency of $N_{cum}(D \geqslant 1$ km$) = (1.44 \pm 0.12) * 10^{-3}$ km^{-2}.

3.1.2. Chang'E 5: Summary of Recommended Revision

Our crater measurement for the Chang'E 5 reference unit results in a crater size–frequency distribution representing a crater population of a single emplacement event that provides the cumulative calibration-crater frequency of $N_{cum}(D \geqslant 1$ km$) = (1.44 \pm 0.12) * 10^{-3}$ km^{-2}. One of the recent, high-precision ages of several collected basalt grains have an age of 2030 ± 4 Ma (Li et al. 2021), which is supported by 1963 ± 57 Ma (Che et al. 2021).

3.2. Apollo 12

Apollo 12 touched down in Mare Cognitum located in the southeastern Oceanus Procellarum. Eratosthenian-aged basaltic lava covers the region. A detailed geological map by Iqbal et al. (2020) highlights several flows postdating the nearby high-lands. Major restrictions for the outline of the reference unit for crater statistics are the secondary crater clusters and rays, most

prominently from Copernicus Crater. Neukum et al. (1973), Neukum (1983) used Apollo 12 basaltic samples and crater statistics originally to define two calibration points, for both the early and late lunar history. In this section, we focus on the cratering-chronology model related to the early lunar history. We discuss neither the age of Copernicus Crater (e.g., Neukum & König 1976) nor any related new crater statistics (e.g., Hiesinger et al. 2012; Iqbal et al. 2020).

3.2.1. Apollo 12: Crater Statistics Review and New Results

Figure 4 shows the count unit, crater map, and observed CSFD. The measured craters cover a diameter range between 0.1 and 2 km. We use the diameters larger than 200 m to determine the site-related calibration-crater frequency, as the lower end of the range relates to possible equilibrium saturation and image resolution. The CSFD reveals one resurfacing event indicated by a shift with respect to a proposed isochron near a crater diameter of about 0.95 km. This large-diameter end of the range is populated by four craters, which are survivors of the resurfacing event. They can be identified by their obvious lava embayment and by being the largest craters in the map, as similarly reported by Hiesinger et al. (2002). The crater frequency for the surviving, unfilled crater population is $N_{cum}(D \geqslant 1$ km$) \approx 8.18 * 10^{-3}$ km^{-2}, which could indicate the relative age of the now lava-buried previous surface. For the diameter range between 0.2 and 0.9 km, we observed an undisturbed CSFD that provides the calibration frequency of $N_{cum}(D \geqslant 1$ km$) = (2.34 \pm 0.05) * 10^{-3}$ km^{-2}, when corrected for excess large craters (Werner et al. 2009).

Based on counts by Neukum & König (1976); Neukum & Horn (1976) discussed two populations of craters over a larger area showing higher variability in terms of crater morphology, spatial distribution, and albedo. They interpreted the low crater frequency to be likely representative of a resurfacing event,
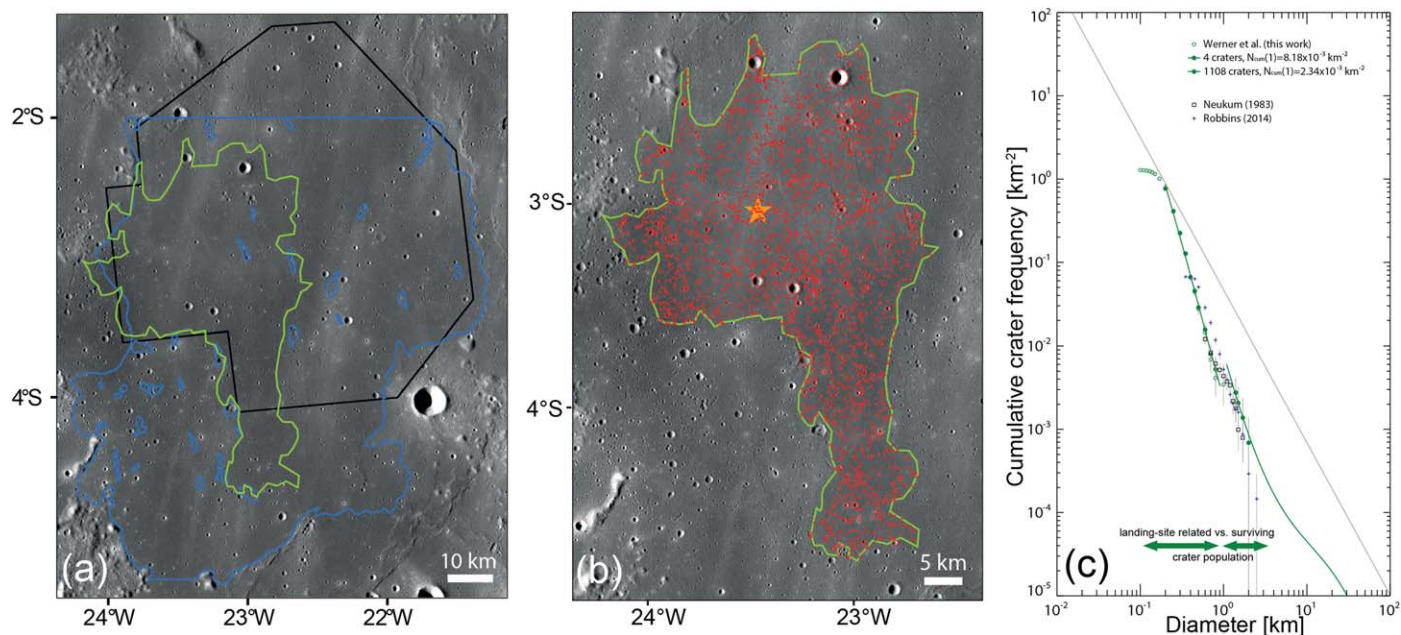
Figure 4. Crater statistics at the Apollo 12 site unit. (a) Comparison of various counting units (green, Werner et al. and this work; black, Neukum & König 1976; blue, Robbins 2014). (b) Counting unit with craters following. (c) The resulting crater size–frequency distributions.

while the high crater frequency corresponds to an older stratum. Neukum et al. (1975) used the low crater frequency of $N_{cum}(D \geqslant 1\,\text{km}) \approx 2.5 * 10^{-3}\,\text{km}^{-2}$, also reported by Wilhelms (1987), to date the youngest lava flooding event. For calibration, they used the youngest sample group age, but they did not attempt to link the higher crater frequency to any older age. Instead, these authors predicted from the higher frequency that the buried material should probably have an age of about 3.6 Ga, but no samples of such an age are part of the collection. The sample ages suggested in the Basaltic Volcanism Study Project (1981) range from 3.08 to 3.24 Ga for the basalts. Since old samples were not found, Neukum (1983) later adjusted the calibration-crater frequency to an average value of $N_{cum}(D \geqslant 1\,\text{km}) = (3.6 \pm 1.1) * 10^{-3}\,\text{km}^{-2}$ and 3.18 ± 0.10 Ga for the age. Robbins (2014) defined an area larger than that of Neukum et al. (1975) and determined a crater frequency of $N_{cum}(D \geqslant 1\,\text{km}) = (5.9 \pm 0.9) * 10^{-3}\,\text{km}^{-2}$, similar to the high value obtained by Neukum & König (1976). Robbins' (2014) measurements show a smooth curve without any resurfacing indication over the entire diameter range between 400 m to 2.5 km. Compared to these previous crater-frequency calibration measurements, the size of $1.45 \times 10^3\,\text{km}^2$ of our Apollo 12 reference unit is about a third or a fifth of the counting units of Neukum (1983) or Robbins (2014), respectively. Because our unit has a smaller areal size, the crater-size range is reduced at the larger diameter but includes smaller craters at the low end due to high-resolution image data.

Our results match well the original result of Neukum & König (1976), and we concur with the suggested lower frequency being representative of the lava coverage, while the higher frequency relates to the previously unflooded stratum. Our frequency values are $N_{cum}(D \geqslant 1\,\text{km}) = (2.34 \pm 0.05) * 10^{-3}\,\text{km}^{-2}$, and $N_{cum}(D \geqslant 1\,\text{km}) = (8.18 \pm 2.3) * 10^{-3}\,\text{km}^{-2}$. We use the lower frequency for calibration of the cratering-chronology model, whereas no sample representative for the higher crater frequency has been identified.

3.2.2. Apollo 12: Summary of Recommended Revision

The crater measurements on the spectrally defined Apollo 12 reference unit result in a CSFD that represents a crater population showing one resurfacing event. Given the stratigraphic setting, we recognize that the lower crater frequency represents the time since lava emplacement. Thus, the fitted isochron provides the cumulative calibration-crater frequency of $N_{cum}(D \geqslant 1\,\text{km}) = (2.34 \pm 0.05) * 10^{-3}\,\text{km}^{-2}$. Although the Apollo 12 basalt samples comprise four distinct types (ilmenite, olivine, pigeonite, and feldspar, Neal et al. 1994), the feldspathic-basalt group spectra match the remote-sensing spectral signature best at and around the actual Apollo 12 landing site (Bultel & Werner 2023). Therefore, we suggest the age of feldspathic basalt sample (12038), which is 3242 ± 13 Ma (Snape et al. 2016), for age calibration of the cratering-chronology model.

3.3. Apollo 15

The Apollo 15 mission landed at the footwalls of the Apennine Mountain front, in the southeastern part of Mare Imbrium. The Apollo 15 reference unit is a lava plain comprising the landing site, limited by the surrounding high-standing Montes Apennine, which are interpreted to be part of the Imbrium Basin rim structure; westwards, it is bound by the Rima Hadley. The cratering-chronology model calibration discussed here focuses on data related to the volcanic plain, not on the age of Imbrium Basin.

3.3.1. Apollo 15: Crater Statistics Review and New Results

We measured the CSFD on a unit that is $3.3 \times 10^2\,\text{km}^2$ in size, somewhat larger than that of Neukum et al. (1975, $2.31 \times 10^2\,\text{km}^2$). Figure 5 shows the outlines of the spectrally identified and morphologically supported unit. For determining the calibration-crater frequency, we measured the craters with respect to diameter and position. We observe a crater population represented by a CSFD that can be described by a
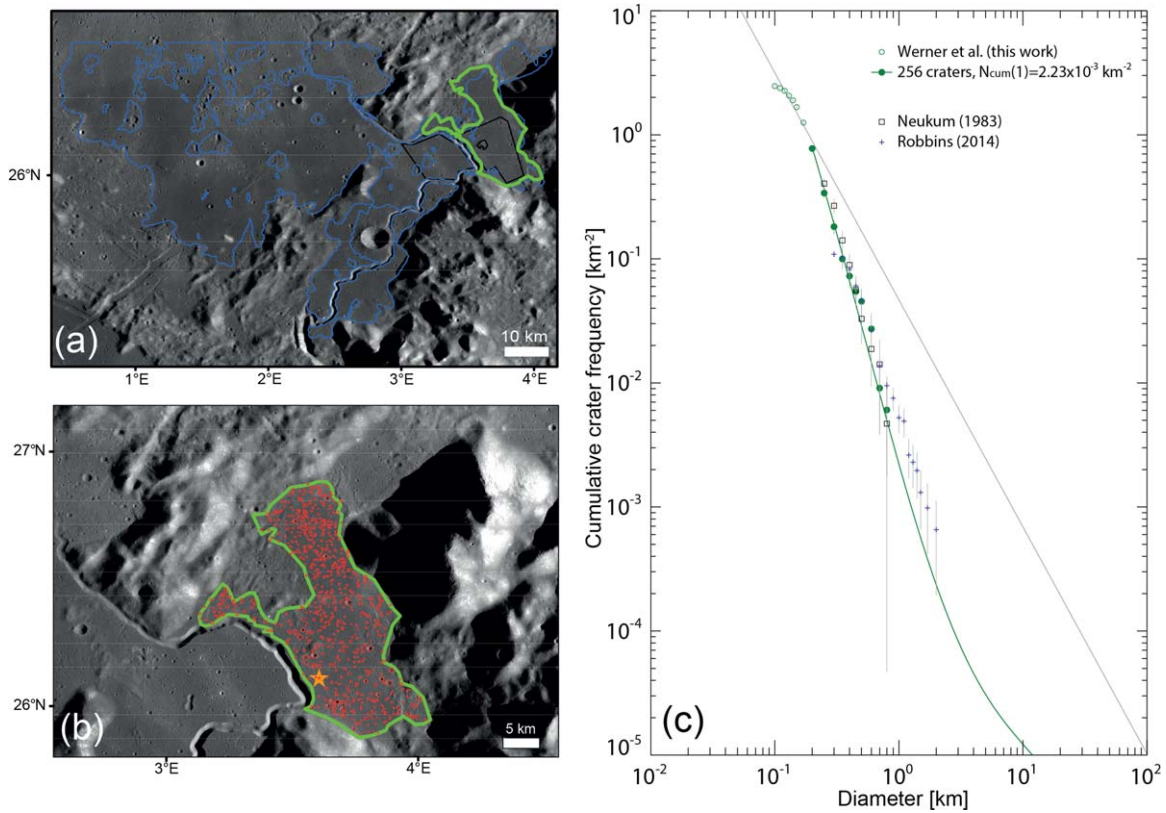
Figure 5. Crater Statistics related to the Apollo 15 landing site. (a) Overview of the counting units: Neukum et al. (1975; used in Neukum 1983) outlined in black, Robbins (2014) in blue, this work in green. (b) The spectrally defined count unit including the marked craters. (c) The resulting crater size–frequency distribution.

single isochron for craters larger than 200 m in diameter, suggesting a single (same age) lava flow covering the Apollo 15 reference unit. The craters below 200 m in diameter approach saturation equilibrium and are therefore excluded from the fit. Earlier studies reported $N_{cum}(D \geqslant 1$ km$) \approx 5.5 * 10^{-3}$ km^{-2} (Marchi et al. 2009; Robbins 2014), $N_{cum}(D \geqslant 1$ km$) \approx 2.6 * 10^{-3}$ km^{-2} (Wilhelms 1987), or $N_{cum}(D \geqslant 1$ km$) \approx 3.2 * 10^{-3}$ km^{-2} (Neukum et al. 1975). The latter provided the original calibration value by Neukum et al. (1975; used in Neukum 1983). Ages for the Apollo 15 samples originally ranged between 3.10 and 3.46 Ga (Basaltic Volcanism Study Project 1981); Neukum (1983) took the average of 3.28 ± 0.1 Ga as the calibration age for the Apollo 15 site.

Robbins (2014) defined a much larger counting area (3.05×10^3 km^2), morphologically identified as mare volcanic plains similar to previous studies (Blewett & Hawke 2001). However, the spectral analyses by Bultel & Werner (2023) revealed compositional differences, clear variations in the number of secondary craters, and additionally large craters that remain unfilled, but are embayed up to the rim by lava flows. These observations in spectral and morphological data contradict the entire mare unit formed at once. This is supported by the fact that Robbins (2014) reports a doubled crater-frequency value compared to Neukum et al. (1975), who studied craters in a small area east of the landing site. Based on our analysis, Robbins (2014) likely included older flows farther to the west. His resulting CSFD exposes a shallower slope than the production function used here and an excess of large craters when compared to our best-fit isochron. For the here-measured CSFD, we determine a

best-fit isochron with a cumulative-crater frequency of $N_{cum}(D \geqslant 1$ km$) = (2.23 \pm 0.12) * 10^{-3}$ km^{-2}.

3.3.2. Apollo 15: Summary of Recommended Revision

The measured CSFD can be fitted with a single isochron that provides the cumulative-crater frequency $N_{cum}(D \geqslant 1$ km$) = (2.23 \pm 0.12) * 10^{-3}$ km^{-2} for the calibration of the cratering-chronology model. For the age calibration, we focus on Apollo 15 samples that relate to the basaltic mare plain. The samples fall into two categories of olivine-normative and quartz-normative basalts. Spectrally, the unit enclosing the landing and sampling sites shows an olivine enrichment (Bultel & Werner 2023); therefore, we propose the respective average age of three low-Ti olivine-normative basalt samples for calibration, which is 3281 ± 12 Ma (Snape et al. 2019).

3.4. Luna 24

In 1976, the last Soviet-Russian robotic mission to sample the Moon landed on the southeast of Crisium Basin in its Late Imbrium mare plains near the craters Fahrenheit and Giordano Bruno. The exact landing site was recognized only later in image data (NAC M119449091LR) of the Lunar Reconnaissance Orbiter. Luna 24 took the deepest coring sample and collected the largest soil sample of all Luna missions.

3.4.1. Luna 24: Crater Statistics Review and New Results

For the crater statistics, the counting unit has a size of 1.30×10^3 km^2. We cover a crater-diameter range of 100 to 1640 m (Figure 6), while previous data sets include craters up
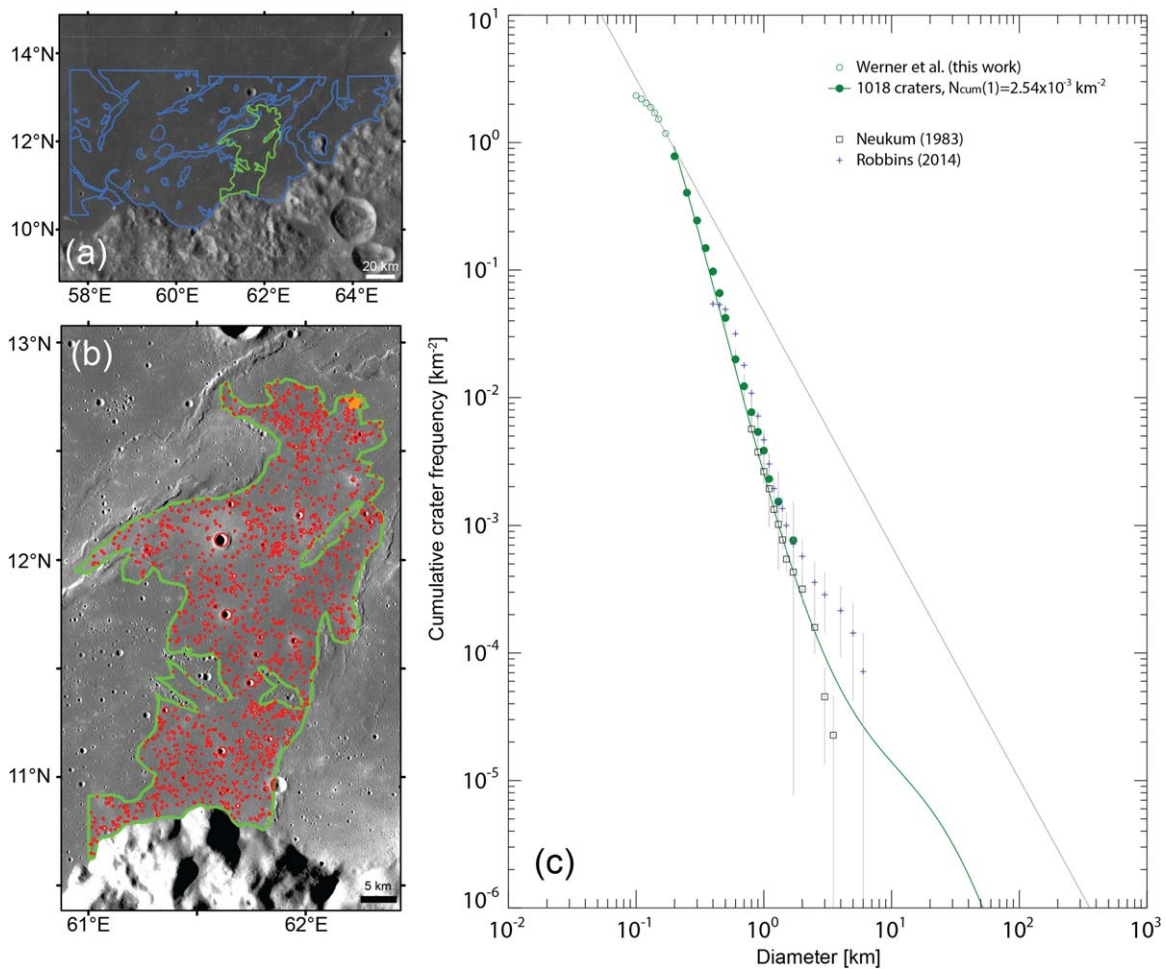
Figure 6. Crater Statistics related to the Luna 24 landing site. (a) Overview of the counting units: Robbins (2014) in blue, this work in green. (b) Our spectrally defined unit including the marked craters. (c) The resulting crater size–frequency distribution.

to about 6 km in diameter reflecting that those studies comprised much larger areas. The unit defined here is about 30 times smaller than that of Neukum et al. (1975) and about a tenth of that of Robbins (2014). We are able to fit a single isochron for craters larger than 200 m; below this diameter, the crater population approaches equilibrium saturation.

The best-fit isochron provides an $N_{\rm cum}(D \geqslant 1$ km$)$ = $(2.54 \pm 0.08) * 10^{-3}\,{\rm km}^{-2}$; which agrees with some previous results $N_{\rm cum}(D \geqslant 1\,{\rm km})$ = $(2.63 \pm 0.24) * 10^{-3}\,{\rm km}^{-2}$ (Neukum et al. 1975). Later, Neukum (1983) reported $N_{\rm cum}(D \geqslant 1$ km$)$ $\approx$ $(3.0 \pm 0.6) * 10^{-3}\,{\rm km}^{-2}$. Robbins (2014) derived $N_{\rm cum}(D \geqslant 1$ km$)$ = $(4.66 \pm 0.58) * 10^{-3}\,{\rm km}^{-2}$, which is almost double compared to ours. The difference between the measurements are the larger area and larger craters, which appear to be relics of incomplete lava emplacement. Correcting for these surviving craters, the measurement of Robbins remains higher compared to our work and previous ones. Based on spectral analysis (Bultel & Werner 2023), we limited the reference unit so that we are certain to study a single lava flow for the Luna 24 landing site, which is supported by the single isochron match to the CSFD. According to the same spectral evaluation, basalt samples containing high-calcium pyroxene and some plagioclase match best with those from the remote-sensing data, a description fitting most samples.

3.4.2. Luna 24: Summary of Recommended Revision

The measured CSFD suggests the cumulative-crater frequency $N_{\rm cum}(D \geqslant 1$ km$)$=$(2.54 \pm 0.08) * 10^{-3}\,{\rm km}^{-2}$ for the calibration of the cratering-chronology model. Previously, the average sample age used by Neukum (1983) was 3.3 Ga. Based on more recent and higher-precision data (Cohen et al. 2001) and after considering the updated ^{40}K decay constant of Renne et al. (2011), we suggest the average age of 3328 ± 21 Ma for the calibration.

3.5. Luna 16

Luna 16 samples were the first to be returned by an uncrewed Russian mission. It landed during the year 1970 in Mare Fecunditatis, the mare lava plain of Late Imbrian age inside the pre-Nectarian Fecunditatis Basin. The region of the landing site is partly covered by secondary craters and ray material formed by the crater Langrenus, and a few others placed ejecta rays nearby. It is possible that minor portions of the collected regolith core stem from these craters. The composition of the core sample displays a diversity of anorthositic soil, brecciated material (rich in plagioclase), and rare anorthosite-norite, but the majority of fragments are of basalt composition.
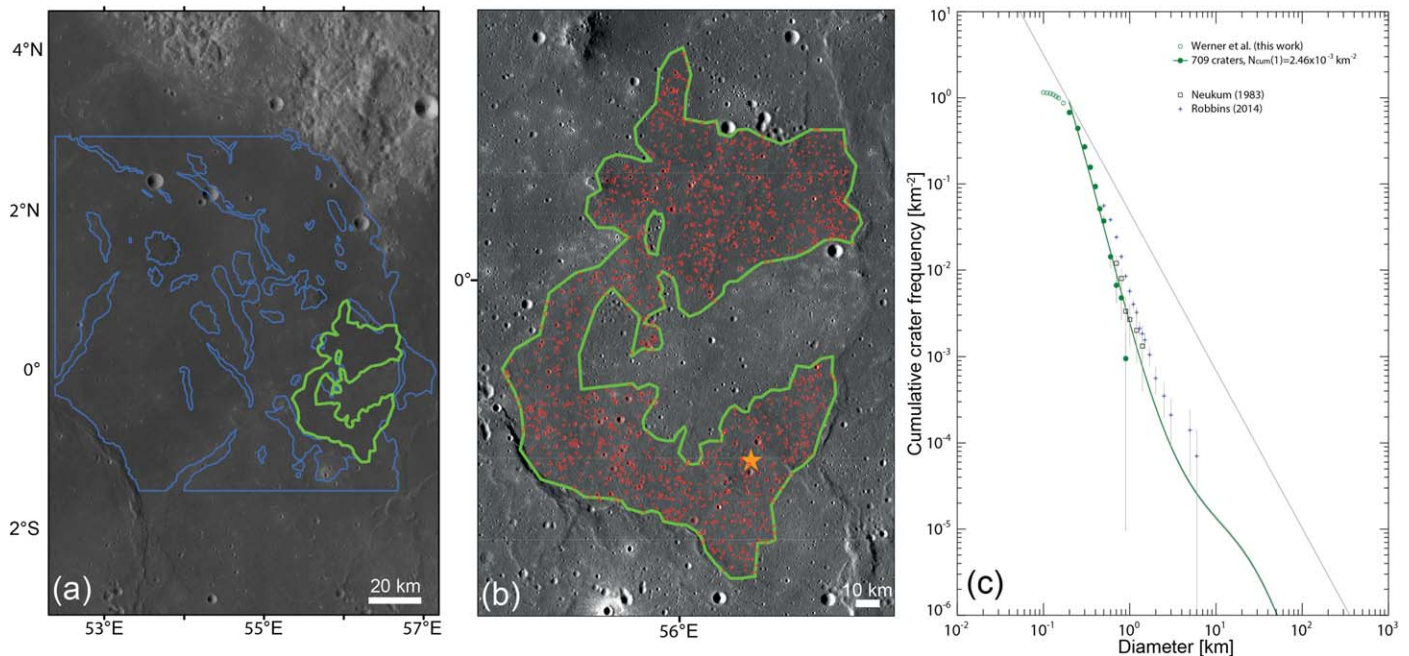
Figure 7. Crater Statistics related to the Luna 16 landing site. (a) Overview of the counting units: Robbins (2014) in blue, Werner et al. (this work) in green. (b) Our spectrally defined count unit including the marked craters. (c) The resulting crater size–frequency distribution.

3.5.1. Luna 16: Crater Statistics Review and New Results

For the crater statistics, the unit has a size of 1.05×10^3 km^2. Compared to previous studies, the unit is similar in size as the one of Neukum (1983) and is roughly a tenth of that of Robbins (2014). We cover a diameter range between 200 and 860 m (Figure 7). For this range, our data set suggests a single-event surface and allows fitting a single isochron to the observed CSFD. Our measurement provides a $N_{\mathrm{cum}}(D \geqslant 1$ km$) = (2.46 \pm 0.09) * 10^{-3}$ km^{-2}, lower than previous results. Neukum (1983) reported $N_{\mathrm{cum}}(D \geqslant 1$ km$) = (3.3 \pm 0.1) * 10^{-3}$ km^{-2} for the representative cumulative frequency, and Robbins (2014) provided $N_{\mathrm{cum}}(D \geqslant 1$ km$) = (5.82 \pm 0.64) * 10^{-3}$ km^{-2}. The latter measurement covers a 10 times larger area and also larger craters. Spectral data by Bultel & Werner (2023) suggest variations across Mare Fecunditatis and within the area outlined by Robbins (2014), morphologically supported by several lava-embayed large craters to be relics of incomplete lava emplacement and the presence of ray materials including secondary craters (the latter are excluded from the count area by Robbins 2014).

3.5.2. Luna 16: Summary of Recommended Revision

The measured CSFD suggests the cumulative-crater frequency $N_{\mathrm{cum}}(D \geqslant 1$ km$) = (2.46 \pm 0.09) * 10^{-3}$ km^{-2} for the calibration of the cratering-chronology model. Previously, the average sample age used by Neukum (1983) was reported to be 3.4 Ga (e.g., Basaltic Volcanism Study Project 1981). The calibration age now corresponds to an updated (using data after Cohen et al. 2001; and the ^{40}K decay constant by Renne et al. 2011) average age of 3382 ± 14 Ma.

3.6. Apollo 11

The Apollo 11 landing site is located at the southwestern edge of Mare Tranquillitatis about 40 km off the nearest highlands. Wilhelms (1987) proposed a stratigraphic sequence with a pre-Nectarian basement, covered by a stack of basin ejecta, and a number of thin layers of Upper Imbrian mare basalt that sealed this column of ejecta. The different lava samples show distinguishable K content and different pyroxene compositions (low-Ca versus high-Ca). The landing area is covered by ray materials originating from several candidate craters formed on highland materials (Theophilus, Tycho, or Alfraganus) or excavated from below the lava by Moltke Crater, about 40 km southeast of the landing site (Korotev & Gillis 2001). The actual landing site is situated between two ejecta rays. The major restrictions for the outline of the reference unit for crater statistics are the ubiquitous secondary crater clusters and rays to be excluded.

3.6.1. Crater Statistics Review and New Results

Figure 8 shows the count unit, crater map, and our observed CSFD and data from previous studies. Our Apollo 11 reference-crater counts were performed on a 7.97×10^2 km^2 sized area, about half the size used by Neukum (Neukum & Horn 1976; interpreted measurements by Shoemaker et al. 1970; Greeley & Gault 1970) and much smaller than the unit of Robbins (2014). Our measurement covers a crater-size range of 0.05–1.2 km in diameter, but we did not analyze craters below 250 m in diameter, because this population appeared to follow the distribution slope of a population in empirical equilibrium (Hartmann 1984). For our measurements, the largest crater observed is 1.2 km in diameter, and is expected for the age and size of the area according to the plotted isochron (Figure 8). Previous measurements contained larger craters, because the considered areas are larger. In the smaller crater diameter range, the different crater size–frequency measurements overlap within uncertainties. Our CSFD measured on a unit defined by morphology and spectrally, unlike previous measurements, displays a smooth distribution representing only the last episode of lava emplacement. Consequently, we fitted only
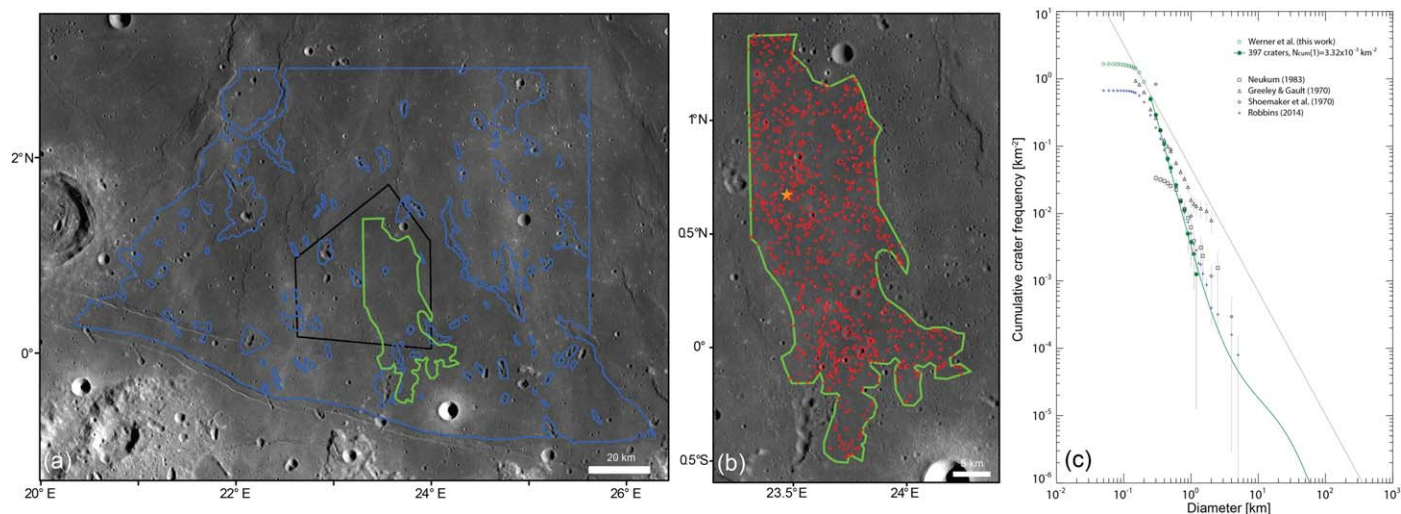
Figure 8. Crater statistics for the Apollo 11 landing area. (a) Overview of the counting units (green, Werner et al., this work; black, Neukum et al. 1975; as used in Neukum 1983; blue, Robbins 2014). (b) Counting unit with craters. (c) The respective crater size–frequency distributions.

one isochron, which we used for the calibration of the chronology model.

Using the crater counts of Shoemaker et al. (1970), Greeley & Gault (1970); Neukum & Horn (1976) originally suggested two different episodes of lava emplacement characterized by low-K and high-K basalt samples, respectively, and captured in two distinct crater frequencies for each emplacement. Neukum & Horn (1976) suggested that the lower crater frequency corresponds to the youngest lava flow, while the higher frequency represents a buried flow population (measured by Shoemaker et al. 1970). Thus, Neukum & Horn (1976) tentatively linked crater frequencies to the youngest age (3.55 Ga) and to the oldest age (3.85 Ga) obtained from the samples. Subsequently, Neukum (1983) measured crater frequencies on Lunar Orbiter data and provided the following two representative frequencies for "old" and "young" Mare Tranquillitatis lava flows, respectively: $N_{cum}(D \geqslant 1 \text{ km}) = (9.0 \pm 1.8) * 10^{-3}$ and $(6.4 \pm 2.0) * 10^{-3} \text{ km}^{-2}$. He further updated the ages to 3.72 ± 0.10 and 3.53 ± 0.05 Ga derived from the age collection in the Basaltic Volcanism Study Project (1981). These ages were averages of two groups of samples that were distinguishable by their amount of potassium (low-K and high-K basalt samples).

Robbins (2014) defined a much larger unit than any previous study and reported a crater frequency of $N_{cum}(D \geqslant 1 \text{ km}) = 8.140 * 10^{-3} \text{ km}^{-2}$. An isochron fit provided $N_{cum}(D \geqslant 1 \text{ km}) = 7.67 * 10^{-3} \text{ km}^{-2}$, which is in accordance with other modern frequencies measured for this landing site (compare for example to counts by Iqbal et al. 2019; for the Neukum 1983 unit resulting in $N_{cum}(D \geqslant 1 \text{ km}) = 6.47 * 10^{-3} \text{ km}^{-2}$). While Iqbal et al. (2019) suggested using this frequency toward the lower sample ages, Robbins (2014) suggested that the crater count refers to the "old" lava flow and provided no frequency toward the young sample ages. However, for previous crater statistics (Neukum 1983; Neukum & Horn 1976; Shoemaker et al. 1970; Greeley & Gault 1970; Robbins 2014), spectroscopic investigation confirmed that the counting areas extend across different lava flows. The large impact crater ejecta allowed the identification of spectrally and, thus, compositionally different materials at a depth, which are not basaltic but highland material.

3.6.2. Apollo 11: Summary of Recommended Revision

The crater measurements on the spectrally defined Apollo 11 reference unit result in a CSFD representing a crater population that is unmodified by resurfacing. Thus, a single isochron can be fitted and provides the cumulative calibration-crater frequency of $N_{cum}(D \geqslant 1 \text{ km}) = 3.32 * 10^{-3} \text{ km}^{-2}$. The spectral characterization (Bultel & Werner 2023), including the stratigraphic interpretation, suggests that samples related to the Apollo 11 group (A) basalts are the closest match to the spectral signature at and around the actual landing site. These high-K basalts are very different to the other basalt types according to Beaty & Albee (1978). A recent, high-precision age for sample (10049) supports that these type-A basalts are the youngest basalts at the Apollo 11 landing site (Snape et al. 2019), which suggests a reference calibration age of 3578 ± 9 Ma.

3.7. Apollo 17

Apollo 17 is the last NASA sample return mission in 1972 and landed in the Taurus–Littrow valley. The Montes Taurus is part of the eastern rim of Serenitatis Basin, although more recently formed basalt plains cover the valley floor. Both the Taurus–Littrow valley floor, and the infill of Mare Serenitatis at large, feature spectrally and morphologically basalt coverage, while the surrounding mountains are of different composition. It is debated whether the samples date the formation of the Serenitatis basin or deposits from other subsequently formed basins. The stratigraphic setting for the Apollo 17 landing site and collected samples therefore comprises the possibility of determining three calibration points. Previous crater counts were performed on large portions of Mare Serenitatis and Taurus–Littrow valley separately, each containing the landing site. But the interpretation is challenging for this site, because secondary craters associated to the Tycho Crater scatter across most parts of the plain, also referred to as Central Cluster (e.g., Neukum & König 1976). In this section, we focus on the basalt plain to define one calibration point for the cratering-chronology model.
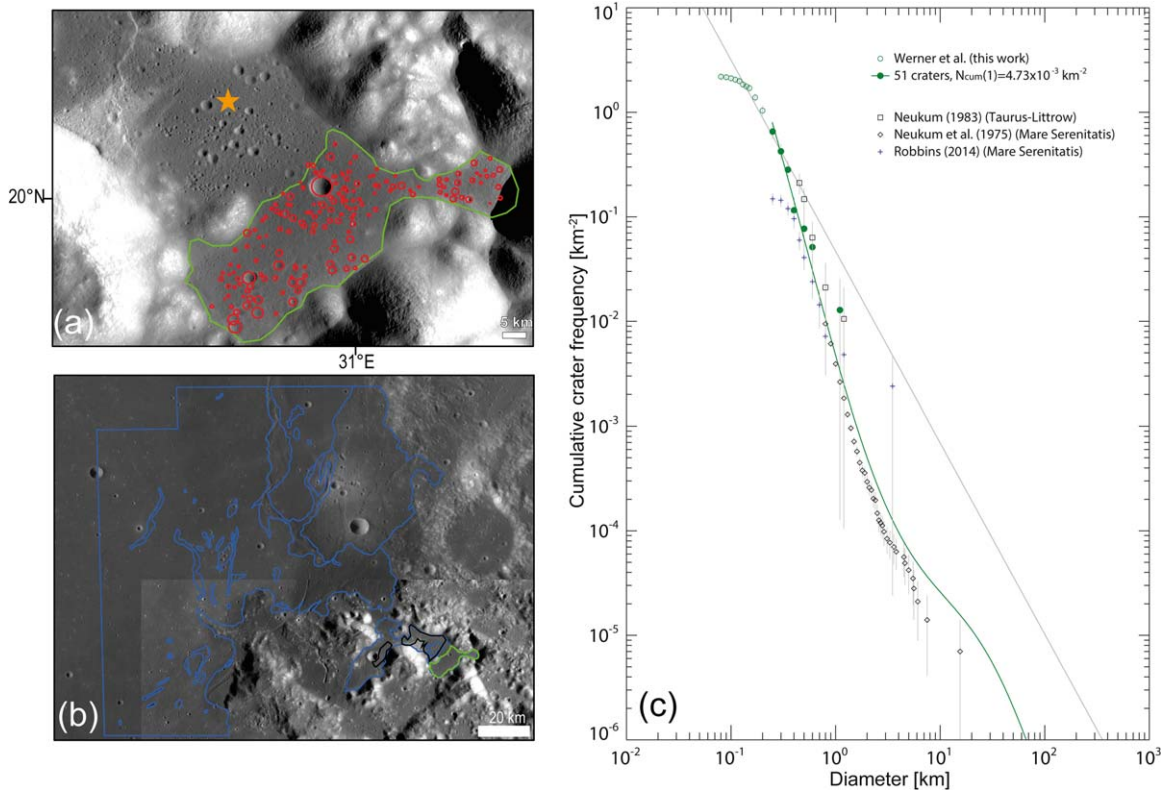
Figure 9. Crater statistics for the Apollo 17 landing area. (a) Spectrally defined counting unit with craters. (b) Overview of counting units (green, Werner et al., this work; black, Neukum 1983; blue, Robbins 2014). (c) The respective crater size frequency distributions.

3.7.1. Apollo 17: Crater Statistics Review and New Results

We measured the CSFD for the Apollo 17 landing site on a unit that is close to 7.8×10^1 km^2 in area, slightly smaller than that used by Neukum et al. (1975, 9.48×10^1 km^2) and about a fifth of the unit Robbins (2014) used. Figure 9 shows the outlines of the spectrally identified unit, excluding the actual landing site, because it is located in one of the secondary crater fields of Tycho. For determining the calibration-crater frequency, we measured the craters with respect to diameter and position in the region of Taurus–Littrow valley, which is the least modified by recent geological activity (landslide, secondary cratering). The crater diameter range covers 80 to 1100 m. We observe a crater population represented by a CSFD matching a single isochron for craters larger than 250 m in diameter, suggesting a single (same age) lava flow covering the Apollo 17 reference unit. The craters below 250 m in diameter appear to be in saturation equilibrium and therefore were excluded for the fit.

Earlier studies reported $N_{cum}(D \geqslant 1 \text{ km}) \approx 3.51 * 10^{-3}$ km^{-2} for the region of Taurus–Littrow valley, and $N_{cum}(D \geqslant 1 \text{ km}) \approx 5.66 * 10^{-3}$ km^{-2} for Mare Serenitatis (Robbins 2014), $N_{cum}(D \geqslant 1 \text{ km}) \approx 9 * 10^{-3}$ km^{-2} (Wilhelms 1987), or $N_{cum}(D \geqslant 1 \text{ km}) \approx 10 * 10^{-3}$ km^{-2} (Neukum 1983) for Mare Serenitatis. Marchi et al. (2009) reinterpreted Neukum's measurement and determined a value as high as $N_{cum}(D \geqslant 1 \text{ km}) \approx 15.8 * 10^{-3}$ km^{-2}, but our fit rather confirms the value $N_{cum}(D \geqslant 1 \text{ km}) \approx 11 * 10^{-3}$ km^{-2} that Neukum (1983) presented for the calibration. However, Neukum et al. (1975) measured also the CSFD for the southern Mare Serenitatis, which is $N_{cum}(D \geqslant 1 \text{ km}) \approx 3.5 * 10^{-3}$ km^{-2} and close to the value found by Robbins (2014) for the Taurus–Littrow valley rather than Mare Serenitatis at large. The crater size–frequency

determined in this study results in a calibration-crater frequency of $N_{cum}(D \geqslant 1 \text{ km}) = 4.73 \pm 0.7 * 10^{-3}$ km^{-2} for a crater diameter range above 300 m related to the apparent saturation equilibrium of the smaller crater population, and the total observed crater range with an upper diameter of 1100 m. Recently revisited by Schmitt et al. (2017), the detailed stratigraphic analysis suggests the Taurus–Littrow valley to be low-lying and older than the adjacent Mare Serenitatis plains in agreement with some previous studies and also this work.

The ages for the Apollo 17 samples associated to volcanic materials of Mare Serenitatis or the Taurus–Littrow valley floor range between 3.59 and 3.84 Ga (Basaltic Volcanism Study Project 1981) of which Neukum (1983) took the average of 3.7 Ga as the calibration age for the Apollo 17 site. The collected Apollo 17 mare samples have similar to higher TiO$_2$ content compared to the Apollo 11 samples and were separated in few types related to their composition. The samples have been interpreted to represent different basaltic lava layers of a stack about 100 m in thickness, with an age range of 3.56 to 3.79 Ga. We used here a spectrally and morphologically identified lava unit, which is distinct from the younger Mare Serenitatis lava plains. Staid et al. (1996) studied the Tranquillitatis region comprising the Apollo 11 and Apollo 17 landing sites and showed that two compositionally distinct mare units exist with expressions in the vicinity of each site. Their work supports that two volcanic episodes may have formed portions of the Maria Serenitatis and Tranquillitatis. Based on our work and the spectral analysis of Bultel & Werner (2023), we characterized the two episodes of which the more recent event is identified at the Apollo 11 site and the earlier one at the Apollo 17 site. Therefore, the likely age for the Apollo 17 reference unit is connected to the presence of olivine,
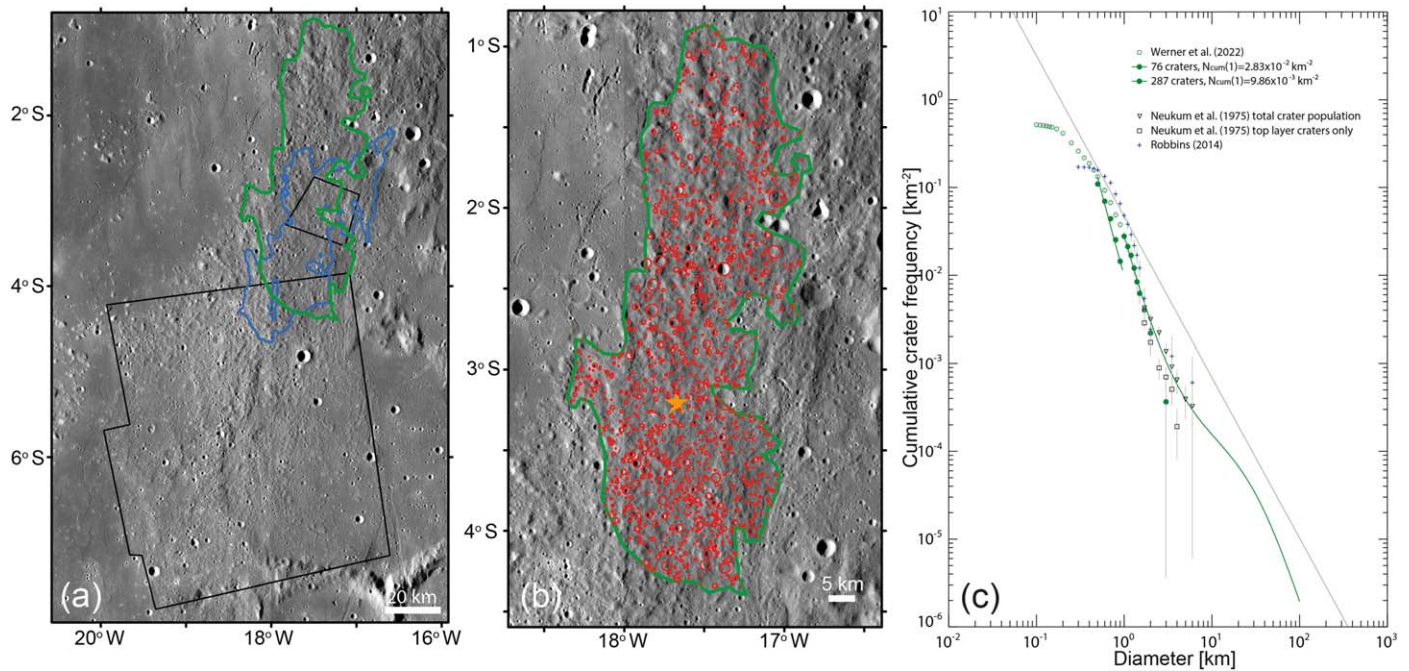
Figure 10. Crater statistics for the Apollo 14 landing area. (a) Overview of the counting units (green, Werner et al., this work; black, Neukum et al. 1975; as used in Neukum 1983; blue, Robbins 2014). (b) Counting unit with craters. (c) The respective crater size–frequency distributions.

plagioclase, and clinopyroxene detected by the remote-sensing spectral mapping and analysis of sample spectra. It thus best corresponds to the description of the samples of basalt group (A). Several ages for this sample group exist, which average to an age of 3753 ± 9 Ma (Snape et al. 2019).

3.7.2. Apollo 17: Summary of Recommended Revision

The measured CSFD can be fitted with a single isochron that provides the cumulative-crater frequency $N_{cum}(D \geqslant 1 \text{ km}) = 4.73 \pm 0.7 * 10^{-3} \text{ km}^{-2}$ for the calibration of the cratering-chronology model. For the age calibration, Apollo 17 group (A) basalt samples match the remote-sensing spectral data best. The average age is 3753 ± 9 Ma (Snape et al. 2019), used as the calibration age in our study.

3.8. Apollo 14

Apollo 14 targeted a landing site about 550 km south of the Imbrium Basin rim near the Fra Mauro Crater. As a stratigraphic formation, this area covered by Imbrium Basin ejecta deposits (Gilbert 1893) accordingly got the name Fra Mauro Formation. The samples comprise a range of impact melt breccia supporting this interpretation. The Apollo 14 reference unit features a hummocky terrain above surrounding the mare. For the calibration of the cratering-chronology model, this site provides two reference points for the early and recent lunar history. Here, we focus on the early history. Since first attempts, the crater counts for this site (compare list by Robbins 2014) and the association of samples as well as sample ages have proven challenging in the past. The entire rock collection sampled at Apollo 14 has a wide range of rock types as well as ages spread between 3.5 Ga to 4.46 (Basaltic Volcanism Study Project 1981).

3.8.1. Apollo 14: Crater Statistics Review and New Results

Werner et al. (2022) collected crater data by diameter and position within the Apollo 14 reference unit. The craters measured at the landing site are smaller than 3 km in diameter, including the about 500 m in diameter Cone Crater, which has been suggested to have formed about 25 million years ago. The Apollo 14 reference unit (Figure 10) has a size of 2.73×10^3 km^2, much smaller than that used by Neukum (1983), but larger than the unit used by Robbins (2014). The measured crater diameter range of 0.2–3 km considered here is less than that in previous work and lacks some larger craters. Compared to isochrons, the observed CSFD exposes a deviation that suggests a resurfacing event removing craters smaller than about 1 km in diameter, a diameter range not investigated by most previous work. However, early work by Neukum et al. (1975) described two relative ages, one relating to the total crater population providing a cumulative-crater frequency $N_{cum}(D \geqslant 1 \text{ km}) = 0.044 \pm 0.003 \text{ km}^{-2}$, and one for a morphologically distinct crater population hosted in a blanketing layer with a cumulative-crater frequency of $N_{cum}(D \geqslant 1 \text{ km}) = 0.020 \pm 0.003 \text{ km}^{-2}$. Later, Neukum (1983) reported an average crater frequency of $0.037 \pm 0.007 \text{ km}^{-2}$ for the relative age of the Fra Mauro Formation and cratering-chronology model calibration. The Robbins (2014) reported crater density $(0.0484 \pm 0.0054 \text{ km}^{-2})$ is the highest of all previously published. The here-adopted cumulative-crater frequencies reported by Werner et al. (2022) are $N_{cum} = 0.028 \pm 0.003$ km^{-2} for the lower strata and 0.0099 ± 0.0008 km^{-2} for the upper strata, respectively. Importantly, only the higher cumulative-crater frequency $N_{cum}(D \geqslant 1 \text{ km}) = 0.028 \pm 0.003$ km^{-2} matches typical relative ages for Imbrium Basin formation. Therefore, the sampled surface and thin uppermost layer at the Apollo 14 landing site are likely not Imbrium ejecta. Werner et al. (2022) proposed it originates from Orientale Basin due to the similarity in relative age (the observed cumulative-crater frequency).
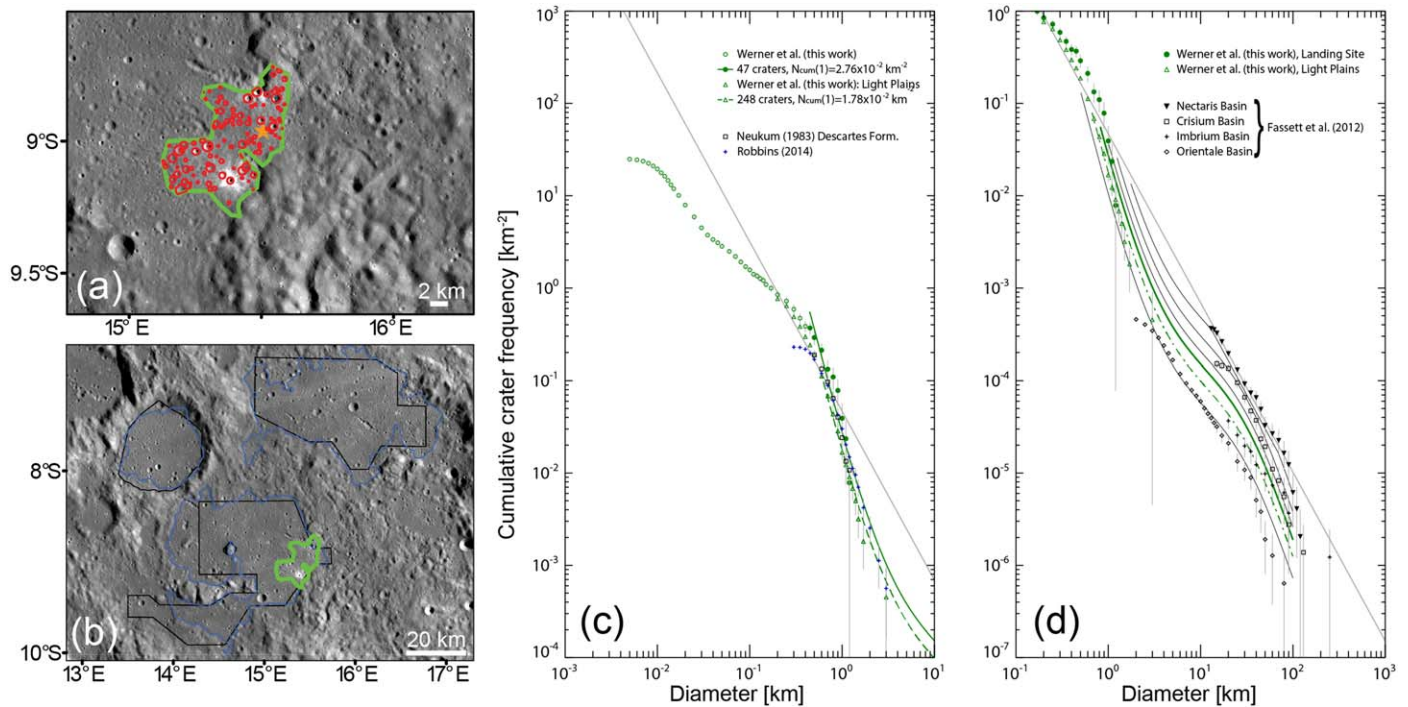
Figure 11. Crater statistics for the Apollo 16 landing area. (a) Our counting unit with craters. (b) Overview of all counting units. (c) The respective crater size–frequency distributions. (d) Apollo 16 in comparison to crater size–frequency distributions (Fassett et al. 2012) for those basins, which likely contributed ejecta to the local stratigraphic column (see Table 1).

3.8.2. Apollo 14: Summary of Recommended Revision

For the cratering-chronology model calibration, we take from Werner et al. (2022) the cumulative-crater frequency of $N_{cum}(D \geqslant 1 \text{ km}) = 0.0099 \pm 0.0008 \text{ km}^{-2}$. The sample spectra matching best the spectral information from the remote-sensing analysis (Werner et al. 2022) provide the relevant samples, which have an average age of 3.922 ± 0.012 Ga (Nemchin et al. 2021), and which is used here for the calibration.

3.9. Apollo 16

Apollo 16 landed in 1972 on the Cayley Plains of suggested Early Imbrian age (Cayley Formation) within the Descartes Mountains constituting the Descartes Formation (Head 1974). Both formations have been suggested to relate to the deposition of ejecta material from one or several impact basins. Alternatively, they can also be composed of material deposited by smaller and nearby impacts rather than basins occurring in the lunar stratigraphy. Seismic data indicates a thickness of the Cayley Formation of about 200 m (Hodges et al. 1973; Cooper et al. 1974). The regolith is suggested to be between 10 and 15 m thick. The samples are mainly brecciated and of impact origin. Both formations may have been sampled at the rims of the craters North Ray (excavation of the Descartes Formation) and South Ray (Cayley Formation). The Descartes Formation is suggested to have been directly sampled being mainly feldspathic breccia (from anorthositic to granulitic) and the most aluminous (James 1982). The samples putatively assigned to the Cayley Formation are mainly mafic impact melt rocks, characterized by very high aluminum and low-K KREEP-component content, potentially delivered from Orientale (Hodges et al. 1973). Morphologically distinct, the Descartes Mountains have been suggested to either by proximity be sourced by Nectaris or consist of Imbrium ejecta (Hodges et al. 1973).

In this section, we focus on the cratering-chronology model calibration related to the early lunar history and discuss neither the age of North Ray Crater (e.g., König et al. 1977) nor any related new crater statistics for it (e.g., Hiesinger et al. 2012).

3.9.1. Apollo 16: Crater Statistics Review and New Results

The crater statistics is performed on a unit that has a size of $1.28 \times 10^2 \text{ km}^2$, half the size compared to Neukum (1983) and much smaller than the unit used by Robbins (2014). This latter work measured an area similar to the Light Plains unit of Neukum et al. (1975), comparable to our extended plains measurement. For the Apollo 16 reference unit, we capture a diameter range between 10 and 1200 m (Figure 11), pushing the low end by almost 2 orders of magnitude compared to those from previous studies. The crater-diameter range documented by Robbins (2014) extends to about 2.9 km, which is natural when a larger area is studied, and agrees with our counts across a large portion of the smooth Cayley Formation plains. The pattern of the CSFD is complex. For the reference unit, we find that the observed CSFD, moving from larger (1.2 km) to smaller crater diameters, shows a shallower slope with respect to the expected production function below 450 m crater diameter, even shallower than the *minus-two* slope typical for cumulative-crater populations of equilibrium or saturated surfaces. Shallowing and saturation are also observed for the extended Cayley-type plains in general (e.g., Xiao & Werner 2015), and supported by our extended plains measurements. The CSFD of the Apollo 16 reference unit below about 450 m reflects loss of small craters, but the craters smaller than 30 m may be overpopulated due to secondary cratering. The range of craters larger than about 450 m matches an isochron resulting in $N_{cum}(D \geqslant 1 \text{ km}) = 2.76 \pm 0.44 * 10^{-2} \text{ km}^{-2}$. Previous results indicate higher frequencies, $N_{cum}(D \geqslant 1 \text{ km}) = 3.4 \pm 0.7 * 10^{-2} \text{ km}^{-2}$ reported by Neukum et al.

(1975), or $N_{cum}(D \geqslant 1$ km$) = 3.1 \pm 0.3 * 10^{-2}$ km^{-2} (Robbins 2014). Both considered a larger counting area made of separate units. However, the separate units show different spectral characteristics, and we therefore follow Bultel & Werner (2023) using a more restricted area in our study.

For a potential interpretation of the crater size–frequency measurements reported here, the basins in the proximity of the landing site that could influence the stratigraphy by their ejecta emplacements are suggested to be as follows: Nectaris, Crisium, Imbrium, and Orientale. Our estimates of the potential layer thickness of the basin ejecta (Table 1) suggest a contribution of Nectaris ejecta of about 1000 m. The emplacement of Nectaris ejecta likely forms the Descartes Formation and not the current surface materials (e.g., Head 1974). For the Descartes Formation, Neukum (1983) related a calibration age of 3.9 Ga for the reported crater frequency of $N_{cum}(D \geqslant 1$ km$) = 3.4 \pm 0.7 * 10^{-2}$ km^{-2}, although it is not fully recoverable where exactly these counts were made. Subsequent contributions to this site could come from Crisium (about 140 m), Imbrium (about 200 m), even Schrödinger (about 1 m), and Orientale (about 10 m). Overall, understanding the stratigraphy at this site is important but challenging. According to Fassett et al. (2012), Nectaris is clearly older, based on the crater density of $N_{cum}(D \geqslant 1$ km$) = 0.0886$ km^{-2}, than the surface observed around the Apollo 16 landing site. The two other candidates with large ejecta contributions at this site have the relative ages $N_{cum}(D \geqslant 1$ km$) = 0.0523$ km^{-2} (Crisium basin-formation age), and $N_{cum}(D \geqslant 1$ km$) = 0.0269$ km^{-2} (Imbrium). The latter coincides with the relative age of the Apollo 16 reference unit. Given the complex pattern of the locally observed CSFD, it is only possible to say that the surface at this site is potentially as old as $N_{cum}(D \geqslant 1$ km$) = 2.76 \pm 0.44 * 10^{-2}$ km^{-2}, but the local material has been reworked steadily since. Despite the limited extent of the reference unit and therefore small number statistics, the relative age of the extended plain is $N_{cum}(D \geqslant 1$ km$) = 1.78 \pm 0.1 * 10^{-2}$ km^{-2}, which does not coincide with any basin-formation age.

Spectrally, the enstatite and plagioclase detections characterize the landing site and its close vicinity. For the stratigraphy, the Cayley Formation comprises materials of a few ejecta layers, which has been gardened into a complex mixture of materials, and the crater record indicates continuous resurfacing. The sample-age range currently covers at least 4.42 to 3.3 Ga or even younger for the glassy samples (Huneke et al. 1973; Turner & Cadogan 1975; Schaeffer & Schaeffer 1977; Maurer et al. 1978; Norman et al. 2003; Fernandes et al. 2013). Some of the breccia samples contain differently aged clasts, or some clasts have partially reset ages within this large age range (Fernandes et al. 2013). Currently, it is not possible to link a single value to the surface for an Apollo 16 calibration age.

3.9.2. Apollo 16: Summary of Recommended Revision

The resulting upper limit for the calibration frequency is $N_{cum}(D \geqslant 1$ km$) = 2.76 \pm 0.44 * 10^{-2}$ km^{-2}, which is lower than the superposed crater frequency for the Nectaris or Crisium basin formation. Unlike earlier suggestions, we do not recommend a calibration frequency. At the current state of knowledge, we consider it impossible to define a calibration age for this site.

3.10. Luna 20

The second robotic Luna mission to successfully sample the Moon landed 1972 on the highlands near the crater Apollonius beyond the Nectarian Crisium Basin at the transition to Mare Fecunditatis. Depending on the interpretation of the Crisium Basin diameter (e.g., Neumann et al. 2015) and the samples, Luna 20 could have landed either on highland crust, basin ejecta including impact melts, or mare materials (Wilhelms 1987; Spudis et al. 1989). Afterwards, it was identified in images that the landing site is clearly located outside the mare plains. The sampled regolith grains are mostly of anorthositic composition although less aluminous than other highland samples. The impact melt and/or mare basalt grains are less abundant and mostly of augitic composition.

3.10.1. Luna 20: Crater Statistics Review and New Results

This landing site has not been used for the calibration of any cratering-chronology model. However, recent work by van der Bogert et al. (2017) used Luna 20 sample ages to support crater statistics-based age results for the formation age of Crisium Basin. For this investigation, we use the outline by Bultel & Werner (2023). The area of the Luna 20 calibration unit is 4.98 x10³ km². Our crater-count results cover a crater-diameter range between 0.2 and 17 km, of which craters above 1.5 km in diameter define the isochron and crater frequency for the calibration of the cratering-chronology model. Fassett et al. (2012) performed measurements at crater diameters above 15 km of the ejecta blanket of the Crisium Basin using a larger area. Previously, Neukum (1983) reported for the Crisium Basin formation a crater frequency of $N_{cum}(D \geqslant 1$ km$) = 5.93 * 10^{-2}$ km^{-2}; similar to our result of $N_{cum}(D \geqslant 1$ km$) = 5.96 \pm 0.8 * 10^{-2}$ km^{-2} for the Luna 20 reference unit, and in good agreement with Fassett et al. (2012) for the Crisium Basin-formation relative age (Figure 12).

The crater record further suggests significant resurfacing for craters below 1.5 km in diameter. The basin-formation sequence suggests contributions (Table 1) after Crisium ejecta from the three youngest, but distant, basins (Imbrium, Schrödinger, and Orientale), which could be of the order of 80 m in total with the majority from Imbrium. However, an 80 m layer is not sufficient to considerably disturb the crater record up to 1.5 km diameter craters, as seen in the CSFD, but could contribute to the sampled regolith material.

Published $^{40}Ar/^{39}Ar$ data presently do not provide a single value for the Luna 20 site age. Spectral data for Luna 20 landing site and vicinity suggest mixing of low and high-Ca pyroxene and comprising a single geologic unit of ejecta material. The sample suite cannot be distinguished according to the orbital spectral analysis and provides only an age range, which is 4309 to 4063 Ma (after Cohen et al. 2001; Swindle et al. 1991 with ages updated for the ^{40}K decay constant; Renne et al. 2011).

3.10.2. Luna 20: Summary of Recommended Revision

The resulting calibration frequency is $N_{cum}(D \geqslant 1$ km$) = 5.96 \pm 0.8 * 10^{-2}$ km^{-2} in agreement with frequencies observed for the Crisium Basin-formation age. Currently, it is not possible to link a single age to the Luna 20 site.
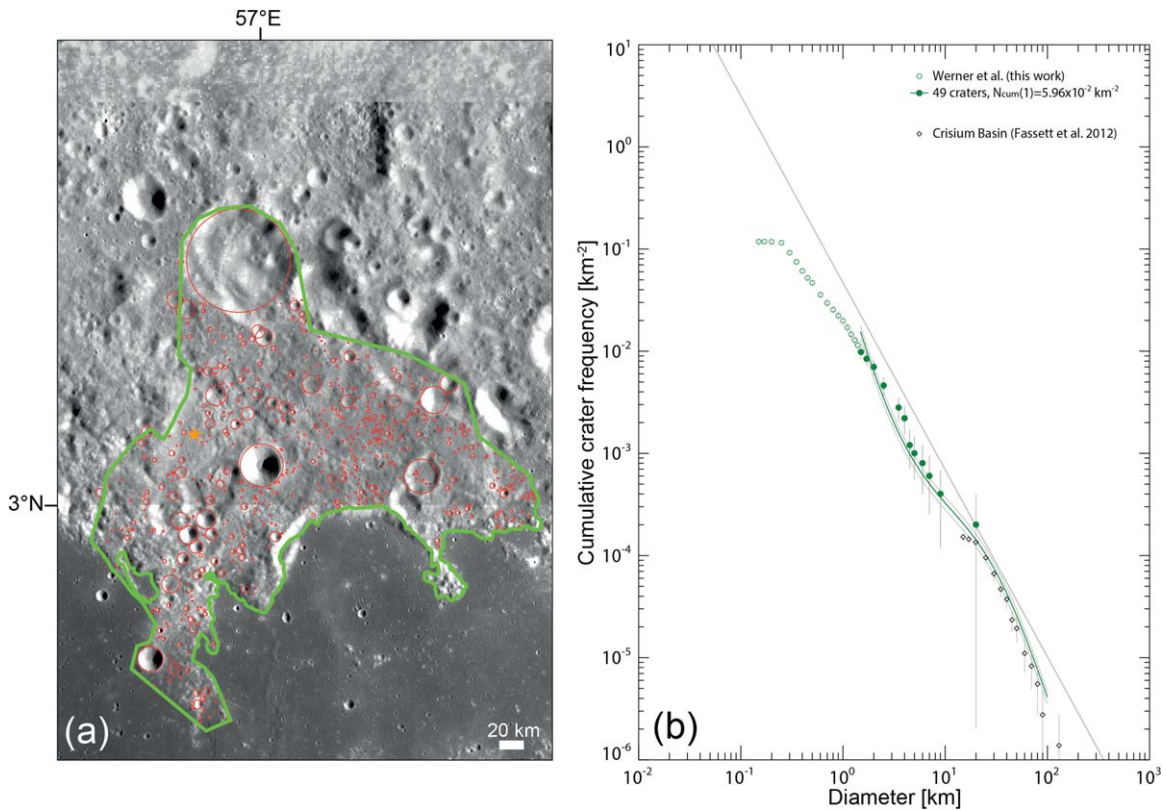
Figure 12. Crater statistics for the Luna 20 landing area. (a) Counting unit with craters. (b) The respective crater-size frequency distribution, and comparison to Crisium superposed crater frequency after Fassett et al. (2012).

3.11. Highlands

Three of the sites (Apollo 14, 16; and Luna 20) are located in the highlands. The observed CSFDs show partial resurfacing and potential reworking of the materials by for example impact gardening in agreement with the wide ranges of sample ages. These landing sites are spectrally characterized by mixed material, probably with diverse provenances. That means, even if crater statistics would be improved, the modification of the crater record is too strong for confirming a relative age. For these sites, we can assume that several basin-forming events delivered materials. The estimates for basin ejecta layer thickness per site are listed in Table 1. While we suggested one of two possible calibration pairs for the Apollo 14 site (see Werner et al. 2022), we cannot provide a recommendation regarding the choice of sample age with respect to the higher Apollo 14 crater frequency nor for the crater frequencies determined for the Apollo 16 or Luna 20 sites at this stage. For Apollo 16 samples, the age range is 3.3 to 4.4 Ga (e.g., Basaltic Volcanism Study Project 1981), and for Luna 20, it is between 4.0 and 4.3 Ga (Cohen et al. 2001; Swindle et al. 1991). The latter is the age range in the case of Luna 20, in the case of limiting the samples to igneous rock texture, but the ages are even younger when breccia materials are included. Considering the complex crater record, impact gardening may further complicate the pairing of samples, which are mostly breccia. No age association and therefore no recommendation of any age can be made for the calibration at this stage. Potentially, a dedicated sample return from bedrock instead of boulders or soils, which may represent materials that have been delivered from elsewhere, would assist in finding an appropriate age for some of the basin-forming events and thus for calibration of the

old range. However, the bedrock samples may have also been reset in age under subsequent impact or lava emplacement events, besides carrying inherited zircons in breccia.

The sample-age record of Apollo 17 includes ages in a range that is much older than that used for the above proposed calibration pair, which correlates to the lava emplacement of Mare Serenitatis. The older ages are mostly for materials with composition different to the Apollo 17 mare material. The range of ages (above 3.8–4.45 Ga) has caused a debate in which it has been speculated what might be the formation age of Serenitatis Basin. Hence, the approach used here provides the crater frequencies for some basin-formation event(s) (Fassett et al. 2012; see also Figure 11), and only defining a calibration pair for the mare lava emplacement.

Following Neukum (1983), we updated the highest observed crater frequency collected for the Moon (i.e., for the Grimaldi Basin-formation age by Fassett et al. 2012) of $N_{cum}(D \geqslant 1 \text{ km})$ $\approx 0.274 \text{ km}^{-2}$, and for the similarly high far side of the Moon as covered by the Zond 8 mission (Ronca et al. 1981). For the corresponding age, we use the oldest zircon age, found in an Apollo 17 sample, suggesting that at least by then the lunar crust has formed and could sustain craters and basins. Another relevant age has been suggested by Nemchin et al. (2009) to be 4417 ± 6 Ma for the fractionation of the KREEP source when forming the lunar crust, which agrees with another ancient age of 4456 ± 40 Ma of the ferroan anorthosite Apollo 16 surfaces rocks (Norman et al. 2003).

3.11.1. Highland: Summary of Recommended Revision

This calibration point does not reflect an actual site, but rather observed peak values, and as such considers the maximal
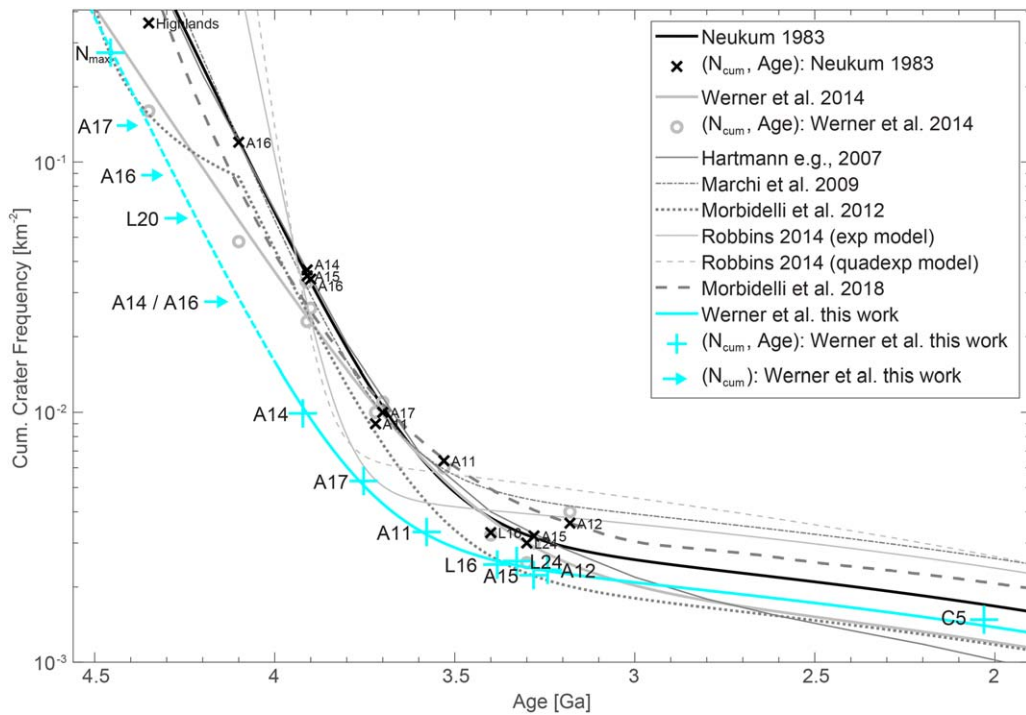
Figure 13. Summary display of the new calibration pairs and the thereof proposed analytical function for the new (cyan) cratering-chronology model together with the standard cratering-chronology calibration (black) by Neukum (1983), and other more recent models (gray).

N_{cum} and age. The resulting calibration frequency is $N_{cum}(D \geqslant 1\ km) = 0.274\ km^{-2}$, and the suggested calibration age is 4456 ± 40 Ma.

4. The Revised Lunar Cratering-Chronology Model

Combining the above-described pairing of site-crater frequencies and related ages, we fit a new analytical function to capture the new cratering-chronology model (represented by an exponential plus constant flux term similarly to Neukum et al. 2001). A summary of the calibration N_{cum}–age pairs for the chronology is listed in supplementary Table 1. In our presentation, we use N_{cum}, which is the normalized cumulative-crater frequency for a defined upper crater diameter determined by counting craters on reference units. These reference units as here presented are mapped using spectral data in relation to sample composition, which provide the assignment of sample ages for the age. The suggested new cratering-chronology model is displayed in Figure 13 together with the current standard cratering-chronology model by Neukum (1983) and others for further discussion. To do this, we essentially revised all pairs for the early phase of lunar bombardment history before 3.2 Ga. We added one calibration pair related to the Chang'E 5 mission at about 2 Ga. We document an observed crater frequency, but lack appropriate calibration ages for the Luna 20, Apollo 16, and the older of two crater frequencies found for Apollo 14 and 17, which have frequencies higher than the Apollo 14 top surface and lower than the highest highland frequencies N_{max}. These five data points without assigned ages stem from the sites of A14 (older, buried surface); A16, which has a similar crater frequency to A14; L20; Nectaris (A16); and Serenitatis (A17) basins. They are indicated by their respective N_{cum} in Figure 13, but currently, we cannot use these for further constraining the cratering-chronology model as discussed above in the respective

sections. Hiesinger et al. (2012) reviewed the calibration pairs for a period younger than about 1 billion years, which are included in our fit of the chronology model (supplementary Figure A2), and support an apparently constant flux since about 3 billion years. The supplementary Figure A2 shows the uncertainty ranges for all N_{cum}–age pairs of the full set of calibration points. For those crater frequency measurements for which we could not confidently assign a specific age (compare arrows in Figure 13), we show the ranges of possible ages, but these should not be confused with age uncertainties (supplementary Figure A2).

The displayed cratering-chronology model that represents the calibration pairs well is in a form that describes the accumulation of craters with time assuming an early monotonically decaying flux (in form of an exponential decay) combined with a constant flux dominant in more recent times. The general shape of the function is $N_{cum}(D \geqslant 1[km]) = a * (exp(b * t) - 1) + c * t$, with a $= 2.9 \times 10^{-14}$, $b = 6.71$, $c = 6.9 \times 10^{-4}$, and t given in Gyrs. We also provide an upper and lower envelope bracketing the crater frequency range, which dominates the uncertainty for deriving the model.

4.1. The New Cratering-Chronology Model in Comparison with Previous Studies

Compared to the often-used standard cratering-chronology model by Neukum (1983), the new model has a similar, monotonic decay rate before 3.5 Ga, but a distinctively lower flux. The here-proposed model suggests lower flux throughout when compared to previous models. This is caused by two necessary updates related to modern sample ages, the effect of differing crater-production functions, and different approaches for outlining the reference unit. Since 1983 (Neukum 1983), both crater statistics and sample ages have been frequently added or revised. One of the more recent comprehensive works

by Robbins (2014) not only mapped and counted craters but also evaluated sample-age assignments, proposing to use the youngest site age as a calibration value. Robbins (2014) already provided a comparison with work by Marchi et al. (2009), Neukum (1983). The actual crater detection and any potential differences in determination of the location and exact diameters are not the reason for the reported differences. Robbins et al. (2014) evaluated the variability of crater diameter identification on identical units and concluded that after some training crater counts agree with an uncertainty of the order of 10%. The models are different, because counts were performed on different units relating the landing sites at which samples were collected, specifically using different image data and how morphological and/or spectral information were used to outline the units. From the different mapping approaches, the identified, assumed homogeneous units differ mostly in size and that changes the covered range of crater diameters and influences the resulting measurements of the CSFD in both shape and frequencies. The identification of the count unit is commonly based on morphological considerations (e.g., Robbins 2014), and until now, only a couple of landing sites were reinvestigated using spectral information (Apollo 11 and 12, Iqbal et al. 2019, 2020).

The representation of the results for defining the chronology model builds on the cumulative density for craters with diameters larger than 1 km. As there are a number of crater-production functions, the observed and the extrapolated values differ and may change the final functional description. This impact has been suggested previously (Werner et al. 2014; Werner & Ivanov 2015), and therefore, we caution that the crater-production function and cratering-chronology model are uniquely linked and not interchangeable. The effect of utilizing differently shaped crater-production functions (e.g., Neukum et al. 2001; Ivanov 2001; Marchi et al. 2009) compared to that used previously (Neukum 1983; Neukum & Ivanov 1994) is shown in Figure 13. The calibration frequencies change significantly; compare, for example, the calibration points by Neukum (1983), Werner et al. (2014). They differ because the latter calibration-crater frequencies were derived by a fit using an updated crater-production function by Ivanov (2001) instead of the one by Neukum (1983). Thus, the here-derived cratering-chronology model is only applicable for the same crater-production function we have used (i.e., Ivanov 2001; Neukum et al. 2001). Moreover, the differently shaped crater-production function is the cause of different calibration frequencies derived by Marchi et al. (2009) despite using the crater size–frequency measurements of Neukum (1983). Robbins (2014) calibration frequencies are direct reads of $N_{cum}(D \geqslant 1\ km)$ for the performed respective measurements and as discussed in the sections above could suffer from (partial) resurfacing events. The modernization of several decades old sample ages, for example, when revised for at least modern decay rates (Michael et al. 2018), further modifies the calibration.

The variations in calibration points due to modern radiometric ages and with the crater densities as presented here does not support several common cratering-chronology model curves (e.g., Hartmann 1970; Neukum 1983; Marchi et al. 2009; Morbidelli et al. 2012; Robbins 2014; Morbidelli et al. 2018). Most prominently, this update suggests a lower cratering rate compared to the original standard cratering-chronology model of Neukum (1983) and most others. As outlined above,

we advocate that the rigorous revision presented here is needed, particularly because of the used spectral characterization for the revising the landing-site reference units, resulting CSFD, and related calibration sample ages using for the sample selection spectral data from remote sensing and samples.

4.2. What About the Period Older Than the Apollo 14 Site or Pre-3.9 Ga Times, Respectively?

Sites such as Luna 20, Apollo 14 and 16 are clearly located in the highlands, but also both Apollo 15 and 17 missions provided samples of highland-compositional affinity. We stated above that for several of the highland sites it is not possible at this stage to derive calibration-age recommendations for the observed crater-frequency values, because the ages of breccia or soils cover a relatively large range. Other challenges relate to the clear absence of identified samples in association to crater statistics, e.g., for the high frequency observed for the Apollo 12 reference unit, which are embayed, surviving craters on the premare emplacement surface. The crater frequency we observe for Luna 20 is in agreement with other studies indicating the relative age for Crisium Basin-formation, but the soil sample ages cover again an ambiguously wide range. The frequency observed for the Apollo 16 reference unit resembles the higher of the two frequencies observed for the Apollo 14 site. Werner et al. (2022) did not recommend a corresponding sample age for the higher frequency since the spectral characteristics of the samples resemble the top layer relating to the lower frequency of the Apollo 14 site. Due to the location of both Apollo 16 and 17, sample ages could reflect the formation of Nectaris or Serenitatis Basin, respectively, although no sample can be linked directly. Again, these ages are diverse for the same sample.

For the Apollo 14, 16, and 17 and the Luna 20 sites, sample ages cover a range between 3.9 Ga to about 4.35 Ga for highland materials and even older ages are recognized for zircon grains included in these highland breccia. Analyses of Apollo 14 breccia (Nemchin et al. 2017; Snape et al. 2018) show that breccia incorporate material of different ages inherited from an unknown source site, especially if long range ejecta must be considered. Therefore, it is impossible to assign any age, or it should be the youngest age found as previous studies already suggested. The latter approach has been followed most recently by Robbins (2014), providing a very late (around 3.9 Ga) and very rapid decay in crater-forming projectile flux, similar to previous interpretations (Tera et al. 1974; Stöffler et al. 1985; Stöffler & Ryder 2001). But this implies that the samples must have formed in situ and ignores that soil is a result of regolith formation including lateral transport or breccia that contain multiple clasts of different age. Both explain the range of ages and ambiguity. However, others suggested that the samples represent only one event globally (Nemchin et al. 2021; Werner et al. 2022), which can be supported by the estimates of ejecta globally deposited across the landing sites.

4.3. Was There a "Lunar Terminal Cataclysm" or "Late Heavy Bombardment"?

From the here-presented data of age and frequency pairs, we can address to some extent whether there was an accumulation of basin-forming events in a specific short period of time. To postulate a *spike* in the bombardment would be due to the

paired values (age and crater statistics) observed at the Apollo 14 and 16 sites, as other samples from the Apollo 15 or 17 collections clearly are materials moved from elsewhere across the lunar surface to the collection site. The question in the latter case would be rather how far the lateral transport of material could have been. However, the ambiguity remains for both the ages and crater statistics. The ambiguity about the age can be explained by the nature of the samples because brecciated material is a conglomerate and shows different ages for the various clasts. Again, one could argue that the youngest measured age in these conglomerates reflects the last event at the source site, but we do not know whether it is a local or distant source. The ambiguity of the crater statistics, however, results from several factors. First, the measurements may be affected by saturation at the studied crater range, but we excluded the range that resembles the saturation slope. Second, the nature of the terrain is such that it is at least partly covered by ejecta material, which makes counting more challenging than on a simple, single lava flow. Finally, the nature of the resurfacing event itself (ejecta deposits) leads to less efficient resurfacing and only partial (if at all) resetting of the sample age, and this leads to increased uncertainty for the paired age—crater-frequency measurement. The frequencies observed at Apollo 14 (buried surface) and Apollo 16 match each other with respect to crater frequency, but suitable samples cannot be unambiguously identified.

Therefore, we suggest that the concept of "lunar terminal cataclysm" in the sense that several basins formed late in a very short time is only a result of the nature of the samples themselves (compare to Nemchin et al. 2021), and furthermore of the nature of the terrain sampled. These terrains have been targets for sampling with the objective of giving ages to the stratigraphic boundary defined by impact basins. In most cases, we found it impossible to recommend an age given the nature of the samples being regolith or breccia, both providing a large range of age in the same sample. However, using the terms *lunar terminal cataclysm* and similarly *late heavy bombardment* rather as concepts define the last large basin-formation event; then Orientale Basin and its extensively spread ejecta defines this event, which is well supported by this study. Samples with Orientale age are predicted to have been collected at Luna 20 and at Apollo 14–17 as also predicted by our pseudo-drill cores. Since at this stage we cannot recommend ages for most of these sites for age calibration, there is only the relative age of all other basins formed before Orientale. Furthermore, the current main constraint is the maximum crater-frequency value for the highlands and a maximum sample age that provides the upper age bound of the lunar solid crust formation. Additional constraints are needed, and for example, the fluxes from the orbital dynamical models or future dedicated sample return may resolve this issue.

5. Conclusion

Currently, the monotonic-flux decay is the best explanation for the here-presented new and revised calibration pairs of crater density and sample age for the sample collection sites of the Apollo, Luna, and Chang'E missions. This new calibration suggests a lower crater-forming projectile flux throughout. Better constraints in age for at least the Luna 20 and Apollo 16

sampling sites would be useful for providing more precise times for individual basin-formation events older than Orientale Basin and to estimate the flux-decay rate better. In any case, the new cratering-chronology model, when transferred to other solid planetary bodies, would cause aging of the surfaces compared to the previous standard models.

Appendix
Supplementary Table and Figures

We have determined crater-size frequencies for the sites from which samples have been collected and returned to Earth. Figure A1 shows the spectral identification maps that display regional variation of the detection criteria as color-composite image for each landing site, which Bultel & Werner (2023) used for outlining the landing-site reference units. The count units used in our investigation demark homogeneous and consistent units based on spectral investigation and define the sample (group) that is the most representative to give the calibration age. In Table A1, we summarize per site the area size of the reference unit, crater fit range, number of craters, the derived cumulative-crater frequencies and error, affiliated age and error, sample number or indicated when it is the average age for a sample group, and the respective reference for the ages we use. Figure A2 shows, similar to Figure 13, the new cratering-chronology model, but now with an uncertainty envelope, as well as the respective calibration pairs with the actual uncertainties for the crater frequencies and assigned ages. Furthermore, we show the age range of samples not assigned for the age calibration, and below one billion years, the calibration pairs stem from Hiesinger et al. (2012). For comparison, the current standard cratering-chronology model by Neukum (1983) is plotted together with other more recent models.
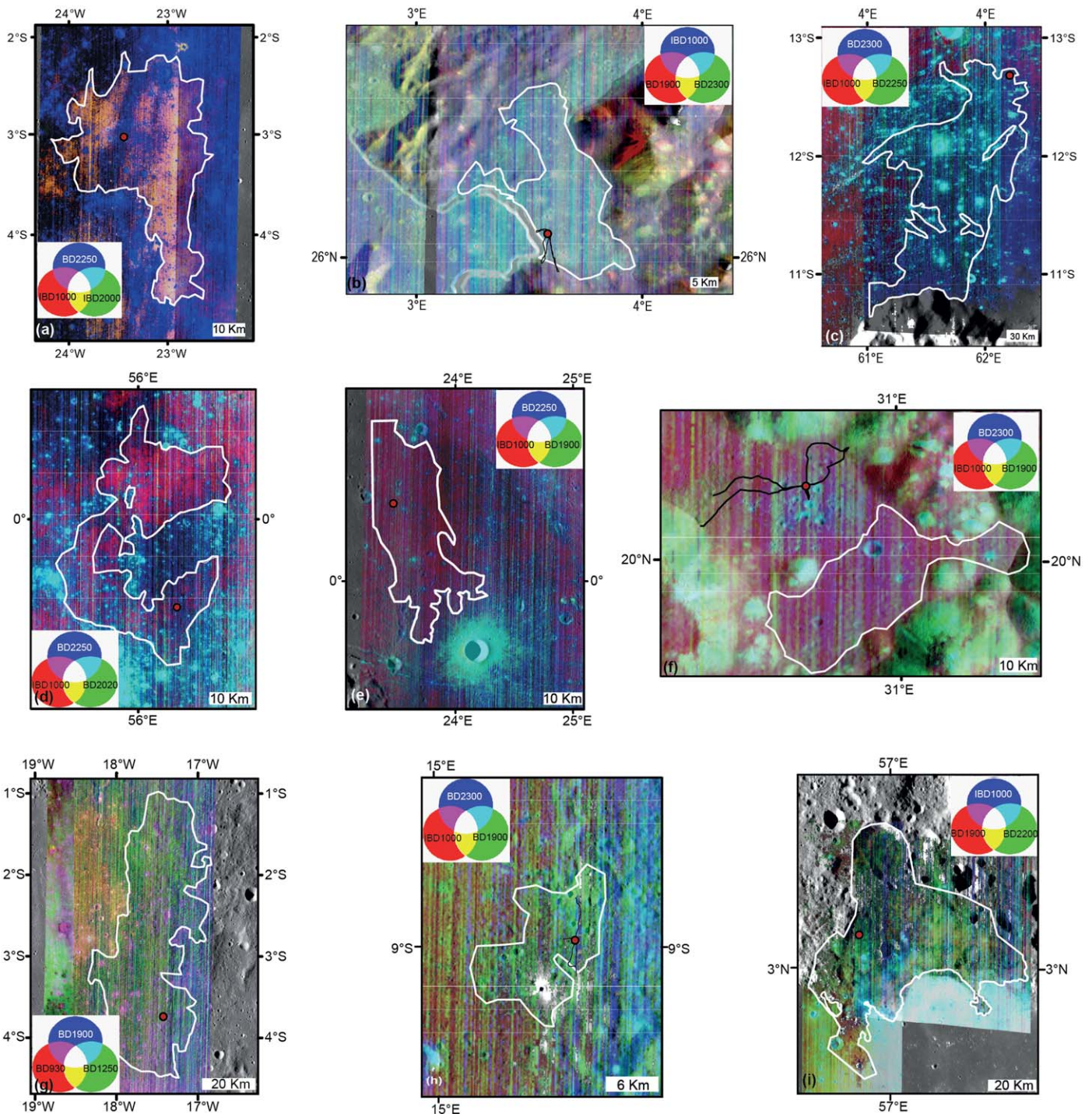
Figure A1. Compilation of the spectral identification color-composite maps and the outlined landing-site reference units used in this work for the determination of crater frequencies. We show the maps for all landing sites for which Luna and Apollo missions sampled the Moon. All the landing-site reference units are outlined in white, all landing sites are localized with a filled red dot, and the astronaut tracks are added in black when the map scale allows for visibility. The color maps are using spectral data collected with the Moon Mineralogical Mapper (M^3) on board the Chandrayaan-1 mission. Data overlay the morphology imaged by the terrain camera (TC) on board the Kaguya mission. The mapping method and spectral criteria details are fully described in Bultel & Werner (2023). Detection according to the spectral criteria is displayed using the red (R), green (G), and blue (B) channels; the specific used criteria are given here for each landing site. (a) Apollo 12 landing site with a color-coded map (R, IBD1000; G, IBD2000; B, BD2250). (b) Apollo 15 (R, BD1900; G, BD2300; B, IBD1000). (c) Luna 24 (R, IBD1000; G, BD2250; B, BD2300). (d) Luna 16 (R, IBD1000; G, BD2020; B, BD2250). (e) Apollo 11 (R, IBD1000; G, BD1900; B, BD2250). (f) Apollo 17 (R, IBD1000; G, BD1900; B, BD2300). (g) Apollo 14 (R, BD930; G, BD1250; B, BD1900). (h) Apollo 16 (R, IBD1000; G, BD1900; B, BD2300). (i) Luna 20 (R, BD1900; G, BD2200; B, IBD1000). Note the Chang'E 5 site is not included, because no spectral analysis was performed.

Table A1
Key Parameters for the Calibration Pairs Used for Deriving the New Cratering-Chronology Model

Site	Regional Affiliation	Area	Fit Range		Craters	N_{cum}	Error	Age	Error	Sample	Age Reference
			D_{min}	D_{max}	No.	($D \geqslant 1$ km)					
		10^3 (km^2)	(m)	(m)		10^{-3} (km^{-2})	10^{-3} (km^{-2})	(Ma)	(Ma)		
Chang'E 5	North Oceanus Procellarum	0.10	150	500	134	1.44	± 0.12	2030	±4	average	Li et al. (2021)
Apollo 12	Mare Cognitum	1.45	200	900	1108	2.34	±0.05	3242	±13	12038	Snape et al. (2016)
Apollo 12	Subsurface Mare Cognitum	1.45	950	2000	4	8.18	±2.3	>3242-4456	…	…	
Apollo 15	Mare Imbrium	0.33	200	1000	256	2.23	±0.12	3281	±12	average	Snape et al. (2019)
Luna 24	Mare Crisium	1.30	100	1640	1018	2.54	±0.08	3328	±21	average	Cohen et al. (2001) [a]
Luna 16	Mare Fecunditatis	1.05	200	860	709	2.46	±0.09	3382	±14	average	Cohen et al. (2001) [a]
Apollo 11	Mare Tranquillitatis	0.797	250	1200	397	3.32	±0.14	3578	±9	10049	Snape et al. (2019)
Apollo 17	Mare Serenitatis/Taurus–Littrow	0.078	250	1100	51	4.73	±0.7	3753	±9	average	Snape et al. (2019)
Apollo 14	Top Layer	2.73	200	950	287	9.86	±0.8	3922	± 12	average	Nemchin et al. (2021)
Apollo 14	Fra Mauro Fm.	2.73	1000	3000	76	28.3	±3	…	…	…	
Apollo 16	Cayley/Light Plains	1.28	450	1200	47	27.6	±4.4	>3922-4400	…	…	…
Luna 20	Crisium B.	4.98	1500	17000	49	59.6	±8	4060-4300	…	…	Cohen et al. (2001) [a]
Nectaris B.	(Apollo 16)	…	…	…	…	88.6	…	>3922-4400	…	…	…
Serenitatis B.	(Apollo 17)	…	…	…	…	140	…	>3922-4450	…	…	…
Highlands	e.g., Grimaldi B.	…	…	…	…	274	…	4456	±40	67215	Norman et al. (2003)

Note.
[a] The ages by Cohen et al. (2001) are updated for the ^{40}K decay constant by Renne et al. (2011) using the Argon Age Recalculator by Mercer (2017).
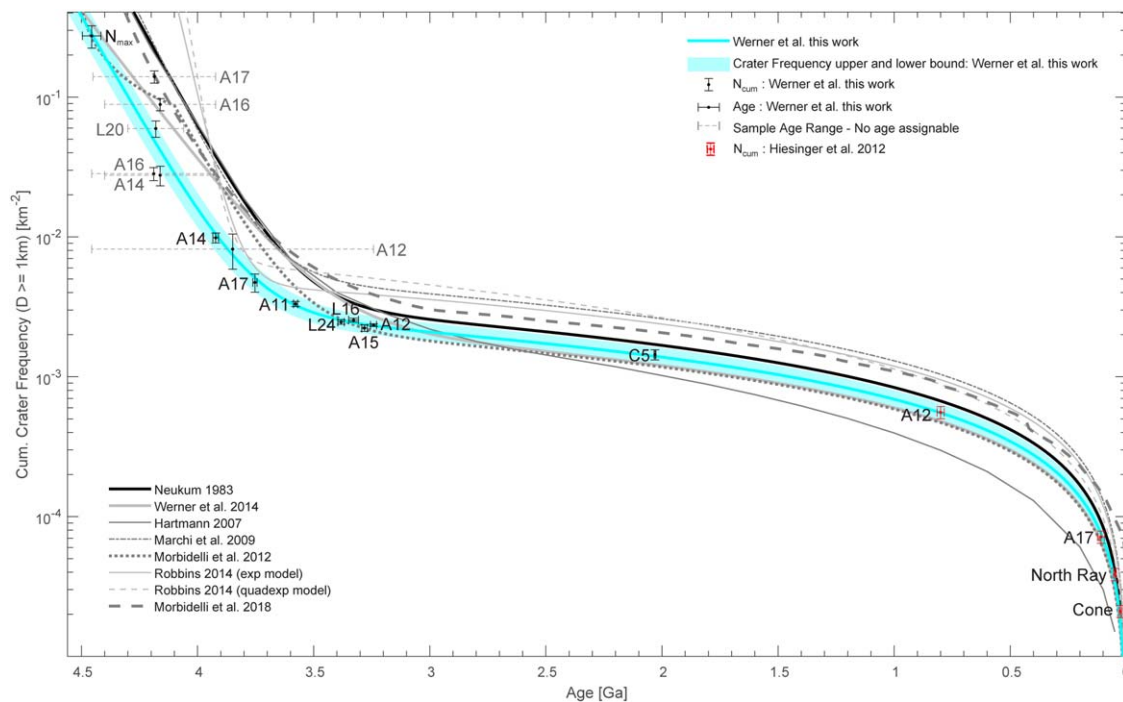
Figure A2. Summary display of the new calibration pairs and the thereof proposed analytical function for the new (cyan) cratering-chronology model. The respective calibration pairs are shown here with uncertainties in the crater frequency and assigned age. The upper and lower bound envelope is so that the calibration uncertainties are captured. Furthermore, we show the age range of samples in cases, for which we have not assigned an age for the calibration. At the young range (below one billion years), calibration pairs marked in red stem from Hiesinger et al. (2012). The current standard cratering-chronology model by Neukum (1983) is plotted (black) together with other more recent models (gray).

ORCID iDs

Stephanie C. Werner ⓘ https://orcid.org/0000-0001-5704-0909
Benjamin Bultel ⓘ https://orcid.org/0000-0002-7084-9574
Tobias Rolf ⓘ https://orcid.org/0000-0003-2252-2451

References

Arvidson, R., Drozd, R. J., Hohenberg, C. M., et al. 1975, Moon, 13, 67
Beaty, D. W., & Albee, A. L. 1978, LPSC, 9, 359
Blewett, D. T., & Hawke, B. R. 2001, M&PS, 36, 701
Bultel, B., & Werner, S. C. 2023, PSJ, 4, 146
Basaltic Volcanism Study Project 1981, Basaltic Volcanism on the Terrestrial Planets (New York: Pergamon)
Che, X., Nemchin, A., Liu, D., et al. 2021, Sci, 374, 887
Cohen, B. A., Snyder, G. A., Hall, C. M., et al. 2001, M&PS, 36, 1345
Cooper, M. R., Kovach, R. L., & Watkins, J. S. 1974, RvGeo, 12, 291
Crater Analysis Techniques Working Group 1979, Icar, 37, 467
Farley, K. A., Malespin, C., Mahaffy, P., et al. 2014, Sci, 343, 1247166
Fassett, C. I., Head, J. W., Kadish, S. J., et al. 2012, JGRE, 117, E00H06
Fassett, C., Head, J., Smith, D., et al. 2011, GeoRL, 38, L17201
Fernandes, V. A., Fritz, J., Weiss, B., et al. 2013, M&PS, 48, 241
Fritz, J., Bitsch, B., Kührt, E., et al. 2014, P&SS, 98, 254
Gilbert, G. K. 1893, Phil. Soc. Washington Bull, 12, 452
Gillis, J. J., Jolliff, B. L., & Korotev, R. L. 2004, GeCoA, 68, 3791
Goswami, J. N., & Annadurai, M. 2009, Curr. Sci., 96, 486
Greeley, R., & Gault, D. E. 1970, Moon, 2, 10
Green, R. O., Pieters, C., Mouroulis, P., et al. 2011, JGRE, 116, E00G19
Hartmann, W. K. 1970, Icar, 12, 131
Hartmann, W. K. 1984, Icar, 60, 56
Hartmann, W. K. 2003, M&PS, 38, 579
Hartmann, W. K., Quantin, C., & Mangold, N. 2007, Icar, 186, 11
Haruyama, J., Matsunaga, T., Ohtake, M., et al. 2008, EP&S, 60, 243
Head, J. W. 1974, Moon, 11, 77
Hiesinger, H., Jaumann, R., Neukam, G., & Head, J. W. 2000, JGR, 105, 29239
Hiesinger, H., Head, J. W., Wolf, U., et al. 2002, GeoRL, 29, 1248
Hiesinger, H., van der Bogert, C. H., Pasckert, J. H., et al. 2012, JGRE, 117, E00H10
Hodges, C. A., Muehlberger, W. R., & Ulrich, G. E. 1973, LPSC, 4, 1
Huneke, J. C., Jessberger, E. K., Podosek, F. A., & Wasserburg, G. J. 1973, LPSC, 4, 1725
Iqbal, W., Hiesinger, H., & van der Bogert, C. H. 2019, Icar, 333, 528
Iqbal, W., Hiesinger, H., & van der Bogert, C. H. 2020, Icar, 352, 113991
Ivanov, B. A. 2001, SSRv, 96, 87
Ivanov, B. A. 2017, LPSC, 48, 1870
James, O. B. 1982, LPSC, 12, 209
Jolliff, B. L., Gillis, J. J., Haskin, L. A., et al. 2000, JGR, 105, 4197
Jourdan, F., & Renne, P. R. 2007, GeCoA, 71, 387
Jourdan, F., Verati, C., & Feraud, G. 2006, ChGeo, 231, 177
Korotev, R. L., & Gillis, J. J. 2001, JGRE, 106, 12339
König, B., Neukum, G., & Fechtig, H. 1977, LPSC, 8, 555
Levenberg, K. 1944, QAPMa, 2, 164
Li, Q.-L., Zhou, Q., Liu, Y., et al. 2021, Natur, 600, 54
Marchi, S., Mottola, S., Cremonese, G., et al. 2009, AJ, 137, 4936
Marquardt, D. 1963, SIAM Journal on Applied Mathematics, 11, 431
Maurer, P., Eberhardt, P., Geiss, J., et al. 1978, GeCoA, 42, 1687
Mercer C. M. (2017) ArAR — The Argon Age Recalculator http://group18software.asu.edu/
McGetchin, T. R., Settle, M., & Head, J. W. 1973, E&PSL, 20, 226
Michael, G., Basilevsky, A., & Neukum, G. 2018, Icar, 302, 80
Michael, G., & Neukum, G. 2010, E&PSL, 294, 223
Minster, J. F., Birck, J. L., & Allegre, C. J. 1982, Natur, 300, 414
Morbidelli, A., Marchi, S., Bottke, W. F., & Kring, D. A. 2012, E&PSL, 355, 144
Morbidelli, A., Nesvorny, D., Laurenz, V., et al. 2018, Icar, 305, 262
Neal, C. R., Hacker, M. D., Snyder, G. A., et al. 1994, Metic, 29, 334
Nebel, O., Scherer, E. E., & Mezger, K. 2011, E&PSL, 301, 1
Nemchin, A. A., Pidgeon, R. T., Healy, D., et al. 2009, M&PS, 44, 1717
Nemchin, A. A., Jeon, H., Bellucci, J. J., et al. 2017, GeCoA, 217, 441
Nemchin, A. A., Long, T., Jolliff, B. L., et al. 2021, ChEG, 81, 125683
Neukum, G. 1983, PhD thesis, Universität München
Neukum, G., & Horn, P. 1976, Moon, 15, 205
Neukum, G., & Ivanov, B. A. 1994, in Hazards due to Comets and Asteroids, ed. T. Gehrels, M. S Matthews, & A. Schumann (Tucson, AZ: Univ. Arizona Press), 359
Neukum, G., & König, B. 1976, LPSC, 7, 2867

Neukum, G., Hörz, F., Morrison, D. A., & Hartung, J. B. 1973, LPSC, 4, 3255
Neukum, G., Koenig, B., & Arkani-Hamed, J. 1975, Moon, 12, 201
Neukum, G., Ivanov, B. A., & Hartmann, W. K. 2001, SSRv, 96, 55
Neumann, G. A., Zuber, M. T., Wieczorek, M. A., et al. 2015, SciA, 1, e1500852
Norman, M. D., Borg, L. E., Nyquist, L., & Bogard, D. D. 2003, M&PS, 38, 645
Oberbeck, V. R. 1975, RvGeo, 13, 337
Paige, D. A., Foote, M. C., Greenhagen, B. T., et al. 2010, SSRv, 150, 125
Pieters, C. M., Goswami, J. N., Clark, R. N., et al. 2009, Sci, 326, 568
Qian, Y. Q., Xiao, L., Zhao, S. Y., et al. 2018, JGRE, 123, 1407
Qian, Y., Xiao, L., Wang, Q., et al. 2021, E&PSL, 561, 116855
Renne, P. R., Mundil, R., Balco, G., et al. 2011, GeCoA, 75, 5097
Robbins, S. J. 2014, E&PSL, 403, 188
Robbins, S. J., Antonenko, I., Kirchoff, M. R., et al. 2014, Icar, 234, 109
Rolf, T., Zhu, M.-H., Wünnemann, K., & Werner, S. C. 2017, Icar, 286, 138
Ronca, L. B., Basilevsky, A. T., Krychov, V. P., & Ivanov, B. A. 1981, M&P, 24, 209
Rotenberg, E., Davis, D. W., Amelin, Y., et al. 2012, GeCoA, 85, 41
Schaeffer, G. A., & Schaeffer, O. A. 1977, LPSC, 8, 2253
Schmitt, H. H., Petro, N. E., Wells, R. A., et al. 2017, Icar, 298, 2
Schwarz, W. H., & Trieloff, M. 2007, ChGeo, 242, 218
Schwarz, W. H., Kossert, K., Trieloff, M., et al. 2011, GeCoA, 75, 5094
Shoemaker, E. M., Hait, M. H., Swann, G. A., et al. 1970, Sci, 167, 452
Snape, J. F., Nemchin, A. A., Grange, M. L., et al. 2016, GeCoA, 174, 13
Snape, J. F., Davids, B., Nemchin, A. A., et al. 2018, ChGeo, 482, 101

Snape, J. F., Nemchin, A. A., Whitehouse, M. J., et al. 2019, GeCoA, 266, 29
Spudis, P. D., Hawke, B. R., & Lucey, P. G. 1989, LPSC, 20, 1042
Staid, M. I., Pieters, C. M., & Head, J. W. 1996, JGR, 101, 23213
Steiger, R. H., & Jäger, E. 1977, E&PSL, 36, 359
Stöffler, D., & Ryder, G. 2001, SSRv, 96, 9
Stöffler, D., Bischoff, A., Borchardt, R., et al. 1985, LPSC, 15, 449
Swindle, T. D., Spudis, P. D., Taylor, G. J., et al. 1991, LPSC, 21, 167
Tera, F., Papanastassiou, D. A., & Wasserburg, G. J. 1974, E&PSL, 22, 1
Tian, H.-C., Wang, H., Chen, Y., et al. 2021, Natur, 600, 59
Turner, G., & Cadogan, P. H. 1975, LPSC, 6, 1509
Turner, G., Cadogan, P. H., & Yonge, C. J. 1973, LPSC, 4, 1889
van der Bogert, C. H., Hiesinger, H., Spudis, P., et al. 2017, LPICo, 1988, 6009
Walker, D., Grove, T. L., Longhi, J., et al. 1973, E&PSL, 20, 325
Werner, S. C. 2019, M&PS, 54, 1182
Werner, S. C., & Ivanov, B. A. 2015, in Treatise on Geophysics, ed. G. Schubert (2nd ed.; Amsterdam: Elsevier), 327
Werner, S. C., Ivanov, B. A., & Neukum, G. 2009, Icar, 200, 406
Werner, S. C., Ody, A., & Poulet, F. 2014, Sci, 343, 1343
Werner, S. C., Bultel, B., Rolf, T., & Assis Fernandes, V. 2022, PSJ, 3, 65
Wetherill, G. W. 1975, LPSC, 6, 1539
Wilhelms, D. 1987, The Geologic History of the Moon, Professional Paper 1348, USGS, doi:10.3133/pp1348
Wu, B., Huang, J., Li, Y., Wang, Y., & Peng, J. 2018, JGRE, 123, 3256
Xiao, Z., & Werner, S. C. 2015, JGRE, 120, 2277
Xie, M., Zhu, M.-H., Xiao, Z., et al. 2017, GRL, 44, 10171
Zhu, M.-H., Wu?nnemann, K., & Potter, R. 2015, JGRE, 120, 2118